Future Engineering Journal

Volume 3 | Issue 2 Article 2

Performance Comparison of Several Control Algorithms for Tracking Control of Pantograph Mechanism

Laylaa Mahmoud Eng
MTI university, Laylaa.mahmoud@eng.mti.edu.eg

Mohamed Shamseldin Dr
Future University in Egypt, mohamed.abelbbar@fue.edu.eg

Mohamed Sallam Dr
Helwan University, sallam.mohamed@h-eng.helwan.edu.eg

Abdelghany Mohamed Prof
Higher Engineering Institute, Thebes Academy, (on leave from Helwan University), Cairo, Egypt., Abdelghany.mohamed@thebes.edu.eg

Future Engineering Journal

Journal homepage: https://digitalcommons.aaru.edu.jo/fej/

Performance Comparison of Several Control Algorithms for Tracking Control of Pantograph Mechanism

Layla M EL-Tehewy[a], Mohamed A. Shamseldin[b,*], Mohamed Sallam[c] and A. M. Abdel Ghany[d]

[a]*Mechatronics Engineering Department, MTI University, Cairo, Egypt.*
[b]*Mechanical Engineering Department, Future University in Egypt, Cairo, Egypt.*
[c]*Mechanical Engineering Department, Helwan University, Cairo, Egypt.*
[d]*Higher Engineering Institute, Thebes Academy, (on leave from Helwan University), Cairo, Egypt.*

ARTICLEINFO

Article history:
Received June 2022
Received in revised form Aug. 2022
Accepted Sep. 2022

Keywords:
Pantograph Robot;
Manipulator Dynamics;
Flower Pollination (FP);
Nonlinear PID (NLPID);
Fractional Order PID (FOPID;
Model reference adaptive control (MRAC));
Fuzzy PD+I control.

ABSTRACT

A sort of parallel manipulator known as a pantograph robot mechanism was created primarily for industrial requests that required high precision and satisfied speed. While tracking a chosen trajectory profile requires a powerful controller. Because it has four active robot links and one robot passive link in place of just two links like the open chain does, it can carry more loads than the open chain robot mechanism while maintaining accuracy and stability. The calculated model for a closed chain pantograph robot mechanism presented in this paper takes into account the boundary conditions. For the purpose of simulating the dynamics of the pantograph robot mechanism, an entire MATLAB Simulink has been created. The related Simscape model had been created to verify the pantograph mathematical model that had been provided. Five alternative tracking controllers were also created and improved using the Flower Pollination (FP) algorithm. The PID controller, which is used in many engineering applications, is the first control. An enriched Fractional Order PID (FOPID) controller is the second control. The third control considers an improved Nonlinear conventional PID (NLPID) controller, and the parameters for this controller were likewise determined using (FP) optimization using the useful objective function. Model Reference Adaptive Control (MRAC) with PID Compensator is the fourth control. The Fuzzy PD+I Control is the last and final controller. A comparison of the different control methods was completed. A rectangular trajectory was chosen as the end effector of the pantograph robot's position reference because it displays performance during sharp edges and provides a more accurate study. The proposed controllers were used for this task to analyze the performance. The outcomes demonstrate that the Fuzzy PD+I control outperforms the PID, FOPID, NLPID, and MRAC with PID Compensator controllers in terms of performance. In the case of the Fuzzy PD+I control, the angles end effector has a lower rise time, a satisfied settling time, and low overshoot with good precision.

1. Introduction

Robots were categorized as mobiles and manipulators by Jorge Angeles in [1]. Robots that can move around include Big Dog, a four-legged walking robot, swimming fish robots, flying robots with wings, and more. The manipulators must be set up on stage and are made to access areas with a moving end effector, such as the arm or hand.

A manipulator typically consists of three components: a base, a moving end effector, and some links that attach to and activate the end effector from the base. A base is anything that the manipulator is put on, whether it be a moving or stationary object.

* *Corresponding author.* Tel.: +2-0109-880-7958 E-mail address: mohamed.abdelbbar@fue.edu.eg
Peer review under responsibility of Faculty of Engineering and Technology, Future University in Egypt.

https://digitalcommons.aaru.edu.jo/fej/

A manipulator that may be mounted to a drone's bottom was created by Jonathan Hodgins [5]. For the drones, Moritz Arns created a dual-purpose landing gear [6]. The CANADARM was created to be transported into space and do work [7]. Additionally, the manipulators could be mounted on the fixed base. Industrial robots are positioned along the assembly line to work on the parts that are transported there [8].

The manipulators' structures can be broadly divided into serial and parallel manipulators.

A serial robot has links that are successively connected from the base to the moving end effector. In detail, the open-chain structure had a first link that begins from a fixed base then connected to the remaining links, the last connection is usually where the end effector is mounted. In contradiction of the open-loop construction, a closed-loop mechanism uses numerous kinematic chains to connect the end effector to the fixed base. In the literature, closed-loop structural mechanisms are also known as parallel mechanisms [9].

Serial structures have some drawbacks, including poor location precision and mechanical rigidity. A serial mechanism with many links has a low position accuracy because a little amount of inaccuracy at each joint is magnified and aggregated by its successive linkages. Furthermore, because each link must carry the mass of its future connections and actuators, the mechanical rigidity of the open-loop system is essentially weak [10].

Three revolute joints perpendicular to the plane are used to create a planar serial robot that can move horizontally, longitudinally, and rotate as well [9]. Because of their parallel structure arrangement, parallel manipulators have larger load-structure ratios than their serial counterparts and higher levels of rigidity, stiffness, motion accuracy, speed, and acceleration [11]. In addition, they have no cumulative joint/link error.

Parallel structure mechanisms have piqued the interest of both academics and industry in recent years due to their benefits over serial structure mechanisms. Although the drawbacks of parallel robots have reduced workspace and needful a more convoluted analysis of singularities than serial robots [12]. This type of closed-chain robot of various shapes and types has been developed in several ways and is widely used in a variety of fields, due to their performance characteristics, that's including pick up and placement [13] [14], machinery manufacturing [15] [16] [17] [18], vehicle simulation devices [19], medical devices [20] [21] [22], laser cutting, space applications [23] [24], underground assembly robots, entertainment equipment, micro-instruments [25] [26], and sensor applications. This type of mechanism has aroused our interest due to its many different advantages, as we mentioned earlier.

After lengthy research in this field, it was found that a number of important points were not completely covered, and other points where research and studies were rare. This statement is as follows:

- High Load:

The scarcity or almost non-existence of research that added the load factor to the model with its utmost importance, as the possibility of carrying this type of mechanism for loads is higher than the serial types with more accuracy.

- Appling Singularity:

At this point, a group of researchers came to discuss this point and mentioned the equations that they deduced without applying them to the Simulation model, but we applied them as simpler and easier way and at the same time fulfilled the required purpose in addition to applying them to the simulation model.

- Precise Control:

Very few researchers have applied types of control to the model, as they are limited to between PID and PD and the like.

But in this study more than one more advanced type with the use of a high-efficiency Optimization Technique [27-28]

- External Load Effect:

The external load considers a disturbance to the pantograph which effects on the accuracy so, this study investigates the performance under different control techniques.

in [29] the PID control was applied to the pantograph. The results discuss and display graphs for the five-bar planar manipulator performance are shown in figure 2. But the control was also applied to reach a certain point as (X , Y) coordinate, not on a path as is the case in the above-mentioned studies, in addition to the fact that no values were estimated for the errors to be able to know an accurate percentage of the errors.

In research [30], the structure control design of a five-bar parallel mechanism is disentangled through the use of the Differential Evolution (DE) algorithm DE. Where the values of the PID controller parameters were clarified for both controllers.

In research for the current year 2021 [31], the researcher also used the PID controller and explained by some numbers the percentage of error, but did not use another control to compare the results. It is assumed that the goal here is to show the best results. At first, a certain point was reached by a straight line from the starting point, and this was considered the first trajectory with an extreme error of 17.2%. Then this model was tested using the PID control also, on a circuit-shaped trajectory with a concentrated error of 11%.

Another control strategy has been used in research [32], which is used Quantitative Feedback Theory (QFT Based Controller). It has been mentioned what has been achieved after applying this type of control. QFT-based controller design gave a rise time of 0.37 seconds. No overshooting was observed in the step responses of both the links. In [32] the frequency domain which is based also on a robust control strategy was implemented. Also, [33] used the Modified Robust Dynamic Control on a Diamond parallel robot (MRDC). It had studied three control methods (PD, Robust Dynamic Control.

This paper develops a pantograph mechanism to be more accurate (considering singularity). Also, Use this developed mathematical model to design the control system. Moreover, design advanced control techniques to improve the accuracy and dynamic performance of the pantograph mechanism. A Comparative study between the proposed control technics (PID , FOPID , NLPID , MRAC with PID Compensator and, Fuzzy PD+I) were achieved. An external planner load on the end-effector had applied to investigate and ensure the controllers' performance.

This paper is structured as follows:

Section 2 gives the mathematical model of the pantograph mechanism includes a description of the pantograph and all of its equations, the simulation of the model using MATLAB Simulink, and the verification using Simscabe. Section 3 presents the control techniques used and the optimization technique. Section 4, presents the results of all previous work with no external load, and with it. Section 5 illustrate the conclusions.

2. Mathematical Model of Pantograph

The system consists of five revolute joints (figure 1), two of them are active, and five-light links. Links 1, 2, 3, and 4 are the driving links, link 0 is a passive link. Using the fitting rotation of the triggering links, the distinguishing point e of the system can track the wanted planar trajectory in the region of the working zone

2.1 Direct Robot Kinematics

The direct robot equations of variables x and y using the θ1 and θ4 are defined as follows [34-36]:

$$x_e=L_1 * \text{cosine}(\theta_1)+L_2 * \text{cosine}(\theta_2)=L_3 * \text{cosine}(\theta_3)+L_4 * \text{cosine}(\theta_4)+L_5 \quad (1)$$

$$y_e=L_1 * \text{sine}(\theta_1)+L_2 * \text{sine}\ \theta_2=L_3 * \text{sine}\,\theta_3+L_4 * \text{sine}\ \theta_4 \quad (2)$$

There are two methods, Trigonometry method or Newton-Raphson method can be used to find θ_3 and θ_2 . In this work, the trigonometry technique was utilized to follow:

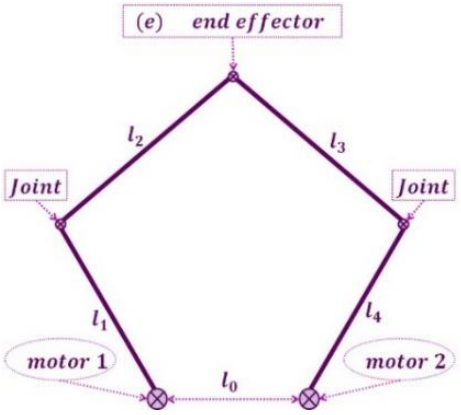

Fig. 1 - Forward Kinematics

$$\theta_3=2*\tan^{-1}\left(\frac{A\pm\sqrt{A^2+B^2-C^2}}{B-C}\right) \quad (3)$$

Where,

$$A = 2\,L_3\,L_4\,\text{sine}\,\theta_4 - 2\,L_1\,L_3\,\text{cosine}\,\theta_1 \quad (4)$$

$$B = 2L_3L_5-2L_1L_3\,\text{cosine}\,\theta_1+2L_4L_3\,\text{cosine}\,\theta_4 \quad (5)$$

$$C=L_1^2-L_2^2+L_3^2+L_4^2+L_5^2-L_1L_4\,\text{sine}\,\theta_1 * \text{sine}\,\theta_4-2L_1L_5\,\text{cosine}\,\theta_1-2L_4L_5\,\text{cosine}\,\theta_4 * \text{cosine}\,\theta_1 \quad (6)$$

And,

$$\theta_2=\text{sine}^{-1}\left(\frac{L_3 * \text{sine}\,\theta_3+L_4 * \text{sine}\,\theta_4-L_1 * \text{sine}\,\theta_1}{L_2}\right) \quad (7)$$

2.2 Inverse Robot Kinematics

The following equations show the direct relationship between the coordinates of the end-effector and link robot lengths to the stimulating angles θ_1 and θ_4 [49]:

$$\theta_1=2\tan^{-1}\left(\frac{-E\pm\sqrt{D^2+E^2-F^2}}{-D-F}\right) \quad (8)$$

Where,

$$D=x_e$$

$$E=y_e$$

$$F=\frac{L_1^2-L_2^2+x_e^2+y_e^2}{2L_1}$$

And

$$\theta_4=2*\tan^{-1}\left(\frac{-H\pm\sqrt{G^2+H^2-I^2}}{-G-I}\right) \quad (9)$$

Where,

$$G = x_e - L_5$$

$$H=y_e$$

$$I=\frac{L_4^2+L_5^2-L_3^2-2x_cL_5+x_e^2+y_e^2}{2L_4}$$

Future Engineering Journal 2 (2022) 2314-7237

The robot's link lengths are taken into account as a constant, making it easier to answer the aforementioned equations. Without knowing θ_2 and θ_3. it is possible to get θ_1 and θ_4 from equations (5) and (6) [36]. The location of the end-effector (x (e)) and its coordinates (y (e)) are the sole inputs required for regulating the five-link mechanism.

2.3 Boundary Conditions of links

It is significant part that is the allowable boundary for a mechanism.

The first boundary is that the links do'nt touch the singularity state throughout the path [50].

For this to be attained Q_5 must not be like to 180 degrees but rather greater.

So, $Q_5 < 180$ shown in figure 2.

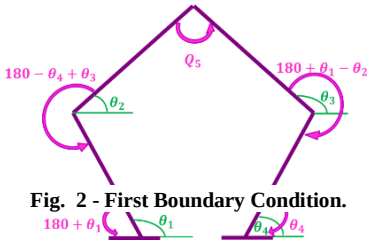

Fig. 2 - First Boundary Condition.

$$Q_5=540-(180+\theta_1)-(180-\theta_4+\theta_3)-(180+\theta_1-\theta_2)-(\theta_4) \quad (10)$$

So the first boundary is:

$$Q_5=(\theta_2-\theta_3)<180 \quad (11)$$

Second one: for the proposed mechanism not to reach the position presented in figure 3, θ_2 must be greater than θ_1 .

Third one: θ_4 must be greater than θ_3.

$(\theta_2>\theta_1)$ (12)

$(\theta_4>\theta_3)$ (13)

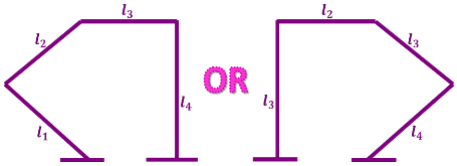

Fig. 3 - Second and Third Boundary Conditions

The three rules (7), (9), and (10), have been implemented by using an easy and simple method on the simulation program (MATLAB Simulink), which is the logic gate (AND), as will be explained in the next.

2.4 Equation of motion:

After defining the forward and inverse kinematics we have to find the position matrix of the center of mass of each link, shown in figure 4, then differentiate it with time to find the velocity for each link, which will be used later.

The equation of motion will be found by using the Lagrangian formulation (equation 14).

$$T = \text{Torque} = \frac{\partial}{\partial t}\frac{\partial L}{\partial \dot{\theta}_i} - \frac{\partial L}{\partial \theta_i} \quad [16] \quad (14)$$

Lagrangian (L) of the system is defined by the mechanism total kinetic energy minus the total system potential energy.

$$L = K - P \quad (15)$$

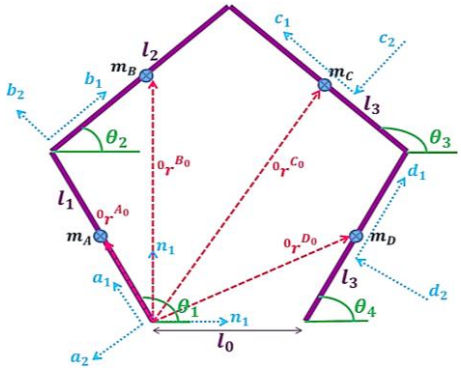

Fig. 4 - Dynamics of the Pantograph

❖ First: determine the total kinetic energy (K) of the system:

- Link L_1 has a rotation motion only

$$K_{L_1} = \frac{1}{2}\frac{m_A {L_1}^2 \dot{\theta_1}^2}{3} = W_1 \dot{\theta_1}^2 \quad (16)$$

- Link L_4 has a rotation motion only

$$K_{L_4} = \frac{1}{2}\frac{m_D {L_4}^2 \dot{\theta_4}^2}{3} = W_2 \dot{\theta_4}^2 \quad (17)$$

- Link L_2 has a translation and rotation motion

$$K_{L_2} = \frac{1}{2}\frac{m_B {L_2}^2 \dot{\theta_2}^2}{12} + \frac{1}{2} m_B ({}^N V^B)^2 = W_3 \dot{\theta_2}^2 + W_4 \dot{\theta_1}^2 + W_5 \dot{\theta_2}^2 + W_6 Z_5 \dot{\theta_1} \dot{\theta_2} \quad (18)$$

- Link L_3 has a translation and rotation motion

$$K_{L_3} = \frac{1}{2}\frac{m_C {L_3}^2 \dot{\theta_3}^2}{12} + \frac{1}{2} m_C ({}^N V^C)^2 = W_7 \dot{\theta_3}^2 + W_8 \dot{\theta_4}^2 + W_9 \dot{\theta_3}^2 + W_{10} Z_6 \dot{\theta_3} \dot{\theta_4} \quad (19)$$

Second: determine the total potential energy (P) of the system:

The potential energy of a system depends on the vertical coordinates of all its particles. Since the system here, all its parts are located at the same height, which means that there is no effect of potential energy, accordingly, it is equal to zero.

- Finally:

$$L = \dot{\theta_1}^2 (W_1 + W_4) + \dot{\theta_4}^2 (W_2 + W_8) + \dot{\theta_1}^2 Z_1^2 (W_3 + W_5) + \dot{\theta_4}^2 Z_2^2 (W_3 + W_5) + \dot{\theta_1}^2 Z_3^2 (W_7 + W_9) + \dot{\theta_4}^2 Z_4^2 (W_7 + W_9) + 2 Z_1 Z_2 \dot{\theta_1} \dot{\theta_4} (W_3 + W_5) + 2 Z_3 Z_4 \dot{\theta_1} \dot{\theta_4} (W_7 + W_9) + W_6 Z_1 Z_5 \dot{\theta_1}^2 + W_6 Z_2 Z_5 \dot{\theta_1} \dot{\theta_4} + (W_7 W_9) \dot{\theta_4} + W_{10} Z_3 Z_6 \dot{\theta_1} \dot{\theta_4} + W_{10} Z_4 Z_6 \dot{\theta_4}^2 \quad (20)$$

By implementing Lagrange equation (17) outlets on the (L) was got, will reach the equation of motion, represented in torque for each motor, T1, and T2, where (A; B;C; D; E; F) are constants.

$$T_1 = \left(A_1 \ddot{\theta}_1 + B_1 \ddot{\theta}_4 + C_1 \dot{\theta}_1 + D_1 \dot{\theta}_4\right) - \left(E_1 \dot{\theta}_1^2 + F_1 \dot{\theta}_4^2 + G_1 \dot{\theta}_1 \dot{\theta}_4\right) \quad (21)$$

$$T_2 = \left(A_2 \ddot{\theta}_1 + B_2 \ddot{\theta}_4 + C_2 \dot{\theta}_1 + D_2 \dot{\theta}_4\right) - \left(E_2 \dot{\theta}_1^2 + F_2 \dot{\theta}_4^2 + G_2 \dot{\theta}_1 \dot{\theta}_4\right) \quad (22)$$

Where,

$$A_1 = 2 (W_1 + W_4) + 2 (W_3 + W_5) Z_1^2 + 2 W_6 Z_1 Z_5 + 2 Z_3^2 (W_7 + W_9) \quad (23)$$

$$B_1 = 2 Z_1 Z_2 (W_3 + W_5) + (W_6 + Z_2 + Z_5) + 2 Z_3 Z_4 (W_7 + W_9) + (W_{10} + Z_3 + Z_6 + Z_3 + Z_6) \quad (24)$$

$$C_1 = 4 (W_3 + W_5) Z_1 \frac{dZ_1}{dt} + 2 W_6 Z_1 \frac{dZ_5}{dt} + 2 W_6 Z_5 \frac{dZ_1}{dt} + 4 (W_7 + W_9) Z_3 \frac{dZ_3}{dt} \quad (25)$$

$$D_1 = 2 (W_3 + W_5) Z_1 \frac{dZ_2}{dt} + 2 (W_3 + W_5) Z_2 \frac{dZ_1}{dt} + W_6 Z_2 \frac{dZ_5}{dt} + W_6 Z_5 \frac{dZ_2}{dt} + 2 (W_7 + W_9) Z_3 \frac{dZ_4}{dt} + W_{10} Z_6 \frac{dZ_3}{dt} \quad (26)$$

$$E_1 = 2 (W_3 + W_5) Z_1 \frac{dZ_1}{d\theta_1} + 2 (W_7 + W_9) Z_3 \frac{dZ_3}{d\theta_1} + W_6 Z_1 \frac{dZ_5}{d\theta_1} + W_6 Z_5 \frac{dZ_1}{d\theta_1} \quad (27)$$

$$F_1 = 2 (W_3 + W_5) Z_2 \frac{dZ_2}{d\theta_1} + 2 (W_7 + W_9) Z_4 \frac{dZ_4}{d\theta_1} + W_{10} Z_4 \frac{dZ_6}{d\theta_1} + W_{10} Z_6 \frac{dZ_4}{d\theta_1} \quad (28)$$

$$G_1 = 2 (W_3 + W_5) Z_1 \frac{dZ_2}{d\theta_1} + 2 (W_3 + W_5) Z_2 \frac{dZ_1}{d\theta_1} + W_6 Z_2 \frac{dZ_5}{d\theta_1} + W_6 Z_5 \frac{dZ_2}{d\theta_1} + 2 (W_7 + W_9) Z_3 \frac{dZ_4}{d\theta_1} + 2 (W_7 + W_9) Z_4 \frac{dZ_3}{d\theta_1} + W_{10} Z_3 \frac{dZ_6}{d\theta_1} + W_{10} Z_6 \frac{dZ_3}{d\theta_1} \quad (29)$$

$$A_2 = 2 (W_3 + W_5) Z_1 Z_2 + W_6 Z_2 Z_5 + 2 (W_7 + W_9) Z_3 Z_4 + W_{10} Z_3 Z_6 \quad (30)$$

$$B_2 = 2 (W_2 + W_8) + 2 (W_3 + W_5) Z_2^2 + 2 (W_7 + W_9) Z_4^2 + (W_{10} + Z_4 + Z_6) \quad (31)$$

$$C_2 = 2 (W_3 + W_5) Z_1 \frac{dZ_2}{dt} + 2 (W_3 + W_5) Z_2 \frac{dZ_1}{dt} + W_6 Z_2 \frac{dZ_5}{dt} + W_6 Z_5 \frac{dZ_2}{dt} + 2 (W_7 + W_9) Z_3 \frac{dZ_4}{dt} + 2 (W_7 + W_9) Z_4 \frac{dZ_3}{dt} + W_{10} Z_3 \frac{dZ_6}{dt} + W_{10} Z_{10} \frac{dZ_3}{dt} \quad (32)$$

$$D_2 = 4 (W_3 + W_5) Z_2 \frac{dZ_2}{dt} + 4 (W_7 + W_9) Z_4 \frac{dZ_4}{dt} + 2 W_{10} Z_4 \frac{dZ_6}{dt} + 2 W_{10} Z_6 \frac{dZ_4}{dt} \quad (33)$$

$$E_2 = 2 (W_3 + W_5) Z_1 \frac{dZ_1}{d\theta_4} + W_6 Z_1 \frac{dZ_5}{d\theta_4} + W_6 Z_5 \frac{dZ_1}{d\theta_4} + 2 (W_7 + W_9) Z_3 \frac{dZ_3}{d\theta_4} \quad (34)$$

$$F_2 = 2 (W_3 + W_5) Z_2 \frac{dZ_2}{d\theta_4} + 2 (W_7 + W_9) Z_4 \frac{dZ_4}{d\theta_4} + W_{10} Z_4 \frac{dZ_6}{d\theta_4} + W_{10} Z_6 \frac{dZ_4}{d\theta_4} \quad (35)$$

Future Engineering Journal 2 (2022) 2314-7237

$$G_2 = 2\,(W_3 + W_5)\,Z_1\frac{dZ_2}{d\theta_4} + 2\,(W_3 + W_5)\,Z_2\frac{dZ_1}{d\theta_4} + W_6\,Z_2\frac{dZ_5}{d\theta_4} + W_6\,Z_5\frac{dZ_5}{d\theta_4} + 2\,(W_7 + W_9)\,Z_3\frac{dZ_4}{d\theta_4} + W_{10}\,Z_6\frac{dZ_3}{d\theta_4} + 2\,(W_7 + W_9)\,Z_4\frac{dZ_3}{d\theta_4} + W_{10}\,Z_3\frac{dZ_6}{d\theta_4} \quad (36)$$

Where,

$$W_1 = \frac{1}{6}\,m_A\,{L_1}^2 \qquad W_2 = \frac{1}{6}\,m_D\,{L_4}^2$$

$$W_3 = \frac{1}{24}\,m_B\,{L_2}^2 \qquad W_4 = \frac{1}{2}\,m_B\,{L_1}^2$$

$$W_5 = \frac{1}{8}\,m_B\,{L_2}^2 \qquad W_6 = \frac{1}{2}\,m_B\,L_1\,L_2$$

$$W_7 = \frac{1}{24}\,m_C\,{L_3}^2 \qquad W_8 = \frac{1}{2}\,m_C\,{L_4}^2$$

$$W_9 = \frac{1}{8}\,m_C\,{L_3}^2 \qquad W_{10} = \frac{1}{4}\,m_C\,L_3\,L_4$$

$$Z_1 = \frac{\partial\,\theta_2}{\partial\,\theta_1} = \frac{L_1 * \text{sine}(\theta_3 - \theta_1)}{L_2 * \text{sine}(\theta_2 - \theta_3)} \qquad Z_2 = \frac{\partial\,\theta_2}{\partial\,\theta_4} = \frac{L_4 * \text{sine}(\theta_4 - \theta_3)}{L_2 * \text{sine}(\theta_2 - \theta_3)}$$

$$Z_3 = \frac{\partial\,\theta_3}{\partial\,\theta_1} = \frac{L_1 * \text{sine}(\theta_2 - \theta_1)}{L_3 * \text{sine}(\theta_2 - \theta_3)} \qquad Z_4 = \frac{\partial\,\theta_3}{\partial\,\theta_4} = \frac{L_4 * \text{sine}(\theta_4 - \theta_2)}{L_3 * \text{sine}(\theta_2 - \theta_3)}$$

$$Z_5 = \text{cosine}(\theta_1 - \theta_2) \qquad Z_6 = \text{cosine}(\theta_3 - \theta_4)$$

3. Control Techniques:

This section covers the theoretical analysis of five distinct control strategies utilized to boost the pantograph mechanism system's performance. The PID controller is the first technique, followed by FOPID control, NLPID control, and a new hybrid approach that combines model reference adaptive control with PID compensator as the second and fourth techniques (modified MRAC). Fuzzy PD+I control with optimization is the fifth strategy.

To achieve the necessary position tracking, all proposed controllers are optimized utilizing flower pollination based on a specific multi objective function to adjust the controller settings in accordance with the error and the change of error. [37-55]

3.1 PID Controller

Due to its simplicity, dependability, and ease of parameter adjustment, the PID controller is used in many engineering domains. The PID controller's transfer function is U(s) = (Kp + Ki/s + Kd.s) E(s). Where Kp, Ki, and kd, respectively, stand for proportional, integral, and differential gains. Each component of a PID controller serves the following purposes: the proportional component lowers the system's error responses to disturbances; the integral component removes steady-state error (ess); and, finally, the derivative component dampens the dynamic response and increases system stability [56]. The Ziegler-Nichols rule [57] is a well-known technique in traditional PID control to determine the appropriate PID controller parameters. We initially determine the plant parameters for open-loop tuning by giving the open-loop system a step input. The step test result is then used to determine the plant parameters K, TD, and T1, as illustrated in Figure 5. When the loop is closed, Ziegler and Nichols advise utilizing the PID controller parameters listed in Table 1. According to the idea of lessening the integral of the absolute error following the application of a step change to the set point, these parameters are used.

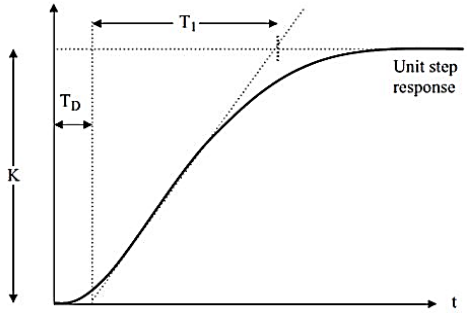

Fig. 5 - system parameters [58].

Table 1 – The open loop system Ziegler/Nichols features [58].

Controller Item	K	T1	TD
(P)	$\frac{T_1}{K\ TD}$	-	-
(PI)	$\frac{0.9\ T_1}{K\ TD}$	3.3 TD	-
(PID)	$\frac{1.2\ T_1}{K\ TD}$	2 TD	0.5 TD

Sometimes the Ziegler-Nichols rule-based conventional PID controller's parameters aren't the greatest. In order to achieve better performance, it can be seen that applying optimization approaches as Flower Pollination Optimization, Genetic Algorithms (GA), Ant Colony Optimization (ACO), and Particle Swarm Optimization (PSO) may result in better PID controller settings [58].

The table 2 below shows the PID parameters following optimization by the flower pollination algorithm.

Table 2 - PID Parameters.

PID Parameters	Kp	Ki	Kd
	20	3	5

3.2 An Optimized Fractional Order Proportional Integral Derivative controller (FOPID)

Mathematics dealing with derivatives and integrals from fractional orders is known as fractional-order calculus. Fractional calculus was rediscovered by engineers and scientists two decades ago, and it is now being used in a growing variety of domains, particularly control theory.

The development of efficient techniques for differentiating from and integrating non-integer order equations has led to the success of fractional-order controllers. Recent years have seen a lot of interest in fractional order proportional-integral-derivative (FOPID) controllers from both an academic and an industrial perspective. In fact, because they have five parameters to choose from, they actually offer more versatility in controller design than do ordinary PID controllers (in place of three). However, this also denotes that the tuning of the controller can be much more complex.

The most public form of a fractional order PID controller is the ($PI^{\lambda}D^{\mu}$), containing an integrator of order λ and a differentiator of order μ, where both (μ & λ) can be any real numbers.

The transfer function of such a controller has the form equation $Gc=(U(s))/(E(s)) = k_p + k_I .1/s^{\lambda} + k_D . s^{\mu}$, ($\lambda$,μ>0) (37)

Figure 6 shows a FOPID block diagram, where Gc(s) is the FOPID controller transfer function, U(s) is the controller output, E(s) is the system error, Kp is the proportional gain, Ki is the integral gain, Kd is the derivative gain, 1/Sλ is the integrator term, Sμ is the differentiator term.

From the FOPID transfer function in equation 9, can notice that:

If (λ=1, and μ=1) a classical PID controller can be achieved, If (λ=1, and μ=0) a PI controller can be realized, If (λ=0, and μ=1) a PD controller can be recovered.

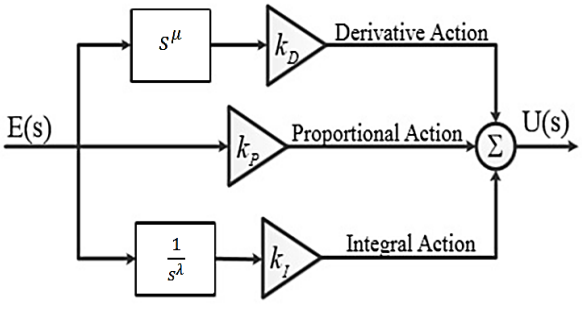

Fig. 6 - FOPID block diagram.

Better control of dynamical systems, which are modelled by fractional-order mathematical equations, is one of the FOPID controller's key advantages. The FOPID controllers' reduced sensitivity to changes in a controlled system's characteristics is another benefit. This is because the two extra degrees of freedom allow a fractional-order control system's dynamical qualities to be adjusted more effectively. The FOPID parameters are optimized by the flower pollination algorithm, its values are shown in table 3 below.

Table 3 - FOPID Parameters

FOPID Parameters	Kp	Ki	Kd	λ	μ
	35	3	15	1.5	0.8

3.3 Non-Linear Proportional Integral Derivative controller (NLPID)

Even though linear fixed parameter PID controllers are frequently suitable for controlling a simple physical process, the requirements for high-performance control with a variety of operating point conditions or environmental parameters are frequently beyond the capabilities of simple PID controllers [59],[60]. The performance of linear PID controllers can be enhanced by using a variety of strategies that were developed to deal with unforeseen disruptions and complex systems, including PID self-tuning approaches, neural networks, fuzzy logic strategies, and other techniques [61],[62],[66],[67],[68],[69].

One of these approaches, called nonlinear PID (NLPID) control, is suggested as the most effective and appropriate for use in industrial applications. There are two main application classes that employ the NLPID control. The first category only applies to nonlinear systems where NLPID control takes care of the nonlinearity. NLPID control is employed in the second category, which deals with simple linear systems, to improve performance that is not possible with a linear PID control, such as reduced overshoot, decreased rise time for the step or rapid command input, obtained better following accuracy, and used to account for the nonlinearity and disturbances in the system [63].

For a quick dynamic reaction and to avoid shaky behavior, the NLPID controllers benefit from having a large initial gain. In order to enhance the performance of a traditional linear PID controller, a sector-bounded nonlinear gain is introduced to a linear fixed gain PID control architecture in this study.

The proposed improved NLPID controller contains two portions. The first portion is a segment bounded nonlinear gain $K_n(e)$ while the second portion is a linear fixed-gain PID controller (K_p, K_i and K_d). The nonlinear gain $K_n(e)$ is a segment-constrained function of the error e(t). The previous research has been considered the nonlinear gain $K_n(e)$ as a one scalar value.

The new in this research, the one scalar value of $K_n(e)$ will be switched with a row vector that can be expressed as $K_n(e) = [K_{n1}(e) \quad K_{n2}(e) \quad K_3(e)]$ as displayed in Figure 7 which will cause humanizing the performance of the NLPID where the values of nonlinear gains will be attuned based on the error and the type of constant parameters (K_p, K_i and K_d).

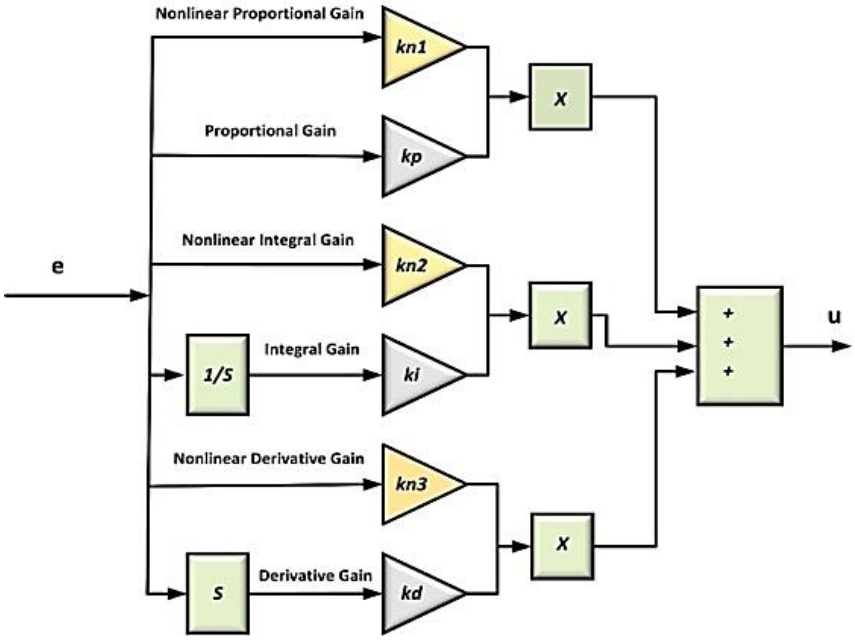

Fig. 7 - The enhanced Nonlinear PID Controller structure.

The proposed form of NLPID control can be described as follows.

$$u(t)=K_p[K_{n1}(e).\ e(t)]+K_i\int_0^t[K_{n2}(e).\ e(t)]\,dt+K_d\left[K_{n3}(e).\ \frac{de(t)}{dt}\right] \quad (38)$$

Future Engineering Journal 2 (2022) 2314-7237

Where $K_{n1}(e), K_{n2}(e)\ and\ K_{n3}(e)$ are nonlinear gains. The nonlinear gains represent any general nonlinear function of the error which is bounded in the sector $0 < K_n(e) < K_n(e)$max.

There is a wide range of choices available for the nonlinear gain $K_n(e)$. One simple form of the nonlinear gain function can be described as.

$$K_{ni}(e) = ch(w_i e) = \frac{\exp(w_i e) + \exp(-w_i e)}{2} \quad (39)$$

Where $i = 1, 2, 3$.

$$e = \begin{cases} e & |e| \le e_{max} \\ e_{max}\,sgn(e) & |e| > e_{max} \end{cases} \quad (40)$$

The nonlinear gain $K_n(e)$ is lower constrained by $K_n(e)$min = 1 when e = 0, and upper-constrained by $K_n(e)$max = ch ($w_i\ e_{max}$). Therefore, e_{max} stand for the range of deviation, and w_i describes the rate of variation of $K_n(e)$.

Selecting the correct parameters to be fitting for the controlled system is the crucial step in PID and NLPID controllers.

There are other methods for determining the PID controller's parameters, such as test/ fault and the Ziegler/Nichols method, although the majority of these are unreliable. The PID and NLPID controllers' optimal settings will be obtained in this thesis using the flower pollination optimization technique. Values of NLPID controllers after optimization by flower pollination algorithm are publicized in table 4 below

Table 4 - NLPID Parameters

NLPID Parameters	Kp	Ki	Kd	W1	W2	W3
	80	3.5	1.3	0.19	3	1.14

3.4 Model Reference Adaptive Control (MRAC)

Model Reference Adaptive Control (MRAC), a high-ranking adaptive controller, describes the needed performance in languages of a reference model that delivers the desired response to a command signal. Figure 8 depicts the elements of a typical MRAC controller, which include a reference model, a control law, and an adaptive mechanism that changes the controller's factors based on the feedback error between the reference model and the actual plant. The main concept of an adaptive controller is to construct a reference model that requires the expected output of the controller, and then the adaptation law modifies the plant's unidentified parameters to achieve zero tracking error [64].

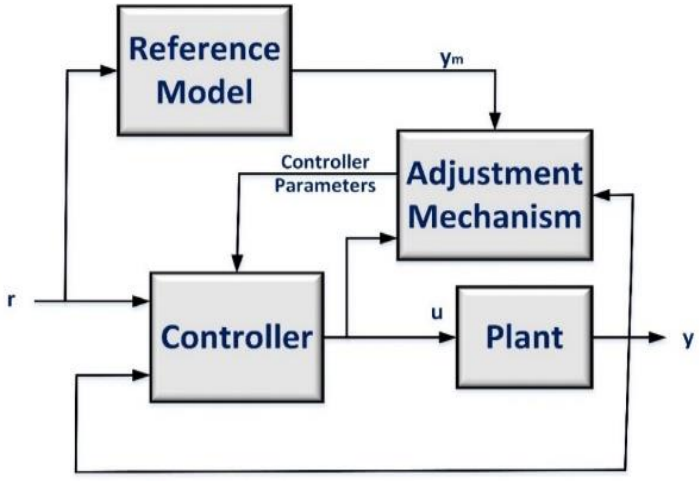

Fig. 8 - A Block diagram of a general MRAC controller [64].

There are two loops in the adaptive controller. A typical feedback controller and the process make up the inner loop. The outer loop modifies the controller's settings so that there is little discrepancy between the model output y_m and process output y, or error, [65].

The original method for model-reference adaptive control was the MIT rule. The name comes from the fact that it was created at MIT's Instrumentation Laboratory, which is now known as the Draper Laboratory. To modify the settings in a way that minimizes the loss function [64],[66.

$$j(\theta) = \frac{1}{2}E^2 \quad (41)$$

To make j small, it is sensible to modification the parameters in the direction of the negative ramp of j, that is,

Future Engineering Journal 2 (2022) 2314-7237

$$\frac{d\theta}{dt} = -\gamma \frac{\partial j}{\partial \theta} = -\gamma E \frac{\partial E}{\partial \theta} \quad (42)$$

Where γ is the adaptation gain, E is the error between the output of the pantograph output and the model reference output ($E = y - y_m$) and θ is the controller parameter as shown in figure 9.

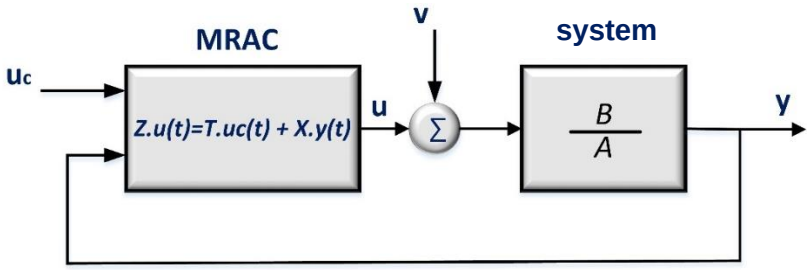

Fig. 9 - A overall linear controller with two marks of freedom.

$$A * y(t) = B * \big(u(t) + v(t)\big) \quad (43)$$

Where A & B: polynomials rely on the system, $u(t)$ is the output of the controller, $y(t)$ is the output of the plant and $v(t)$ is the plant disorder. The controller is defined in (44).

$$Z.u(t) = T.u_c(t) - X.y(t) \quad (44)$$

Where Z, T & X acts the controller parameters polynomials and $u_c(t)$ is the desired angular position.

Substituting (44) into (43) will result in (45)

$$y(t) = \frac{BT}{AZ + BX} u_c(t) + \frac{BZ}{AZ + BX} v(t) \quad (45)$$

Assume that the model reference is termed by the solo-input, solo-output (SISO) system.

$$A_m y_m(t) = B_m u_c(t) \implies y_m(t) = \frac{B_m}{A_m} u_c(t) \quad (46)$$

Where A_m , B_m are the polynomials rely on the reference model, $y_m(t)$ is the output of model reference.

Supposing, ($v(t) = 0$) the subsequent situation must occur:

$$y(t) = y_m(t) \implies \frac{BT}{AZ + BX} = \frac{B_m}{A_m} \quad (47)$$

Suppose that the transfer function of the reference model is

$$\frac{y_m}{u_c} = \frac{b_m}{a_{m1}S^2 + a_{m2}S + a_{m3}} \quad (48)$$

where:

$S = \frac{d}{dt}$.

$a_{m1}, a_{m2}, a_{m3}, b_m$: the model reference transfer function constant.

Suppose that the transfer function of the system is

$$\frac{y}{u} = \frac{b}{a_1 S^2 + a_2 S + a_3} \quad (49)$$

where a_1, a_2, a_3, b: system transfer function coefficient.

From Equation (25) the Diophantine equation is as follows.

$$AZ + BX = A_0 A_m \quad (50)$$

Where:

$A = a_1 S^2 + a_2 S + a_3,\ A_m = a_{m1} S^2 + a_{m2} S + a_{m3}$

A0: Adjustment factor.

$$\deg(X) = \deg(A) - 1 = 2 - 1 = 1$$

where deg is the polynomial degree.

$$X = x_0 + x_1 S \quad (51)$$

$$\deg(Z) = \deg(X) \implies Z = z_0 + z_1 S$$

$$\deg(A_0) = \deg(A) + \deg(R) - \deg(A_m) = 2 + 1 - 2 = 1$$

$$A0 = S \quad (52)$$

Likewise, $T = S$ (53)

Substituting Equations (27, 28 and 29) into Equation (26) will result Equation (30).

$$(z_0 + z_1 S)u = Su_c - (x_1 S + x_0)y \tag{54}$$

$$u = \frac{S}{Z(S)}u_c - \frac{X(S)}{Z(S)}y \tag{55}$$

From Equation (12) and assume $v(t) = 0$

$$(a_1 S^2 + a_2 S + a_3) = bu \tag{56}$$

Substituting (32) into (31) will result in (33)

$$(a_1 S^2 + a_2 S + a_3)y = b\left(\frac{T(S)}{Z(S)}u_c - \frac{X(S)}{Z(S)}y\right)$$
$$\Longrightarrow \left((a_1 S^2 + a_2 S + a_3) + b\frac{X(S)}{Z(S)}\right)y = b\frac{T(S)}{Z(S)}u_c \tag{57}$$

Rewritten (33) to become (34)

$$y = \frac{bT(S)}{(a_1 S^2 + a_2 S + a_3)Z(S) + bS(S)}u_c \tag{58}$$

$$E = y - y_m \tag{59}$$

Substituting Equations (58, 59) into Equation (57) will result in (60)

$$E = \left(\frac{bT(S)}{(a_1 S^2 + a_2 S + a_3)Z(S) + bX(S)} - \frac{b_m}{a_{m1}S^2 + a_{m2}S + a_{m3}}\right)u_c \tag{60}$$

$$\frac{\partial E}{\partial T} = \frac{b}{(a_1 S^2 + a_2 S + a_3)Z(S) + bX(S)}u_c \tag{61}$$

$$\frac{\partial E}{\partial S} = \frac{-b^2 T(S)}{\left((a_1 S^2 + a_2 S + a_3)Z(S) + bX(S)\right)^2}u_c \tag{62}$$

By using Fuzzy control equations

$$\frac{\partial T}{\partial t} = -\gamma E\frac{b}{(a_1 S^2 + a_2 S + a_3)Z(S) + bS(S)}u_c$$

$$\frac{\partial T}{t} = -\gamma' E\frac{1}{(a_1 S^2 + a_2 S + a_3)Z(P) + bX(S)}u_c \tag{63}$$

Where

$$\gamma' = b\gamma \tag{64}$$

Similarly

$$\frac{\partial X}{\partial t} = -\gamma' E\frac{1}{a_{m1}S^2 + a_{m2}S + a_{m3}}y \tag{65}$$

$$\frac{B_m}{A_m} = \frac{{\omega_n}^2}{S^2 + 2\xi\omega_n S + {\omega_n}^2} \tag{66}$$

where:

$\xi\ (damping\ ratio) = 1.$

$\omega_n\ (natural\ frequency) = 500$ rad/sec. (Designated by expert)

Of considerations taken during the design has to be ω_n of a reference model is greater than ω_n of a system transfer function.

3.5 MRAC with PID Compensator

The disadvantages of MRAC may reason high overreaching and high settling time. This difficulty can be assuaged by embracing a PID compensator as presented in Figure 10.

Future Engineering Journal 2 (2022) 2314-7237

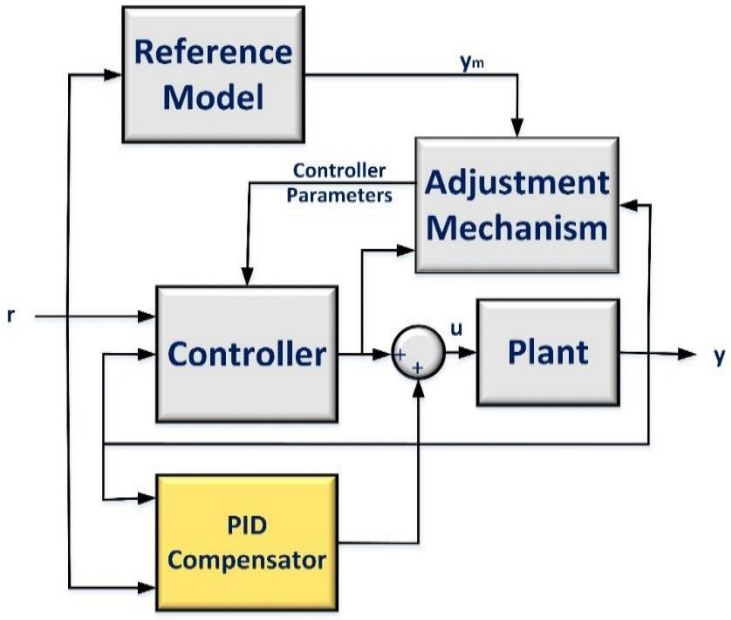

Fig. 10 - Block illustration of MRAC with PID compensator.

The input of the PID compensator is the error between reference speed and actual speed. In this instance, the controller action relies on both the MRAC and the PID compensator as publicized in equation (43). This technique considers a new technique in this thesis.

$$u = u_{MRAC} + u_{PID\ compensator} \quad (67)$$

There are numerous procedures to select the PID compensator parameters such as trial and error and the Ziegler-Nichols rule. In this paper, the parameters of the PID compensator are tuned to give us the best performance.

The parameters of MRAC with PID compensator are shown in table 5 below.

Table 5 - Parameters of MRAC with PID Compensator

PID Parameters	Kp	Ki	Kd
	1300	0.001	70

3.6 Fuzzy Logic PD+I Controller

The over-all construction of fuzzy logic control is denoted in Figure 11 and includes three main components [31].

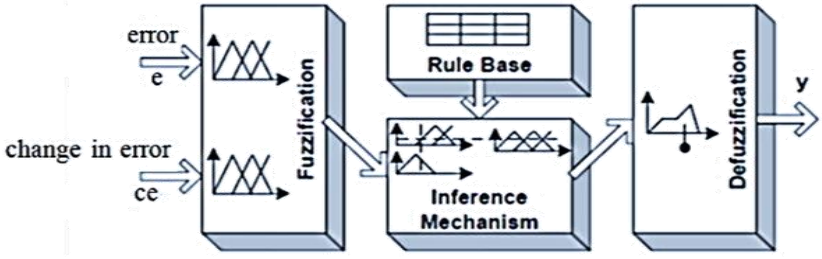

Fig. 11 - Fuzzy logic control construction [57].

Structure of the Fuzzy PD + I controller as shown in figure 12.

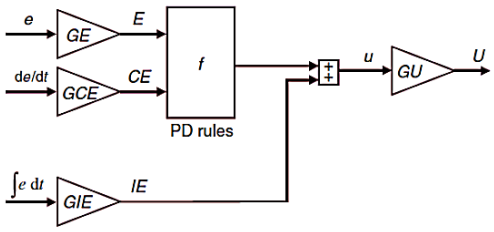

Fig. 12 - Structure of Fuzzy PD+I controller.

To condense, Table 6 shows for each of the four controller's kinds the connections between the PID tuning parameters and fuzzy gain factors useable for fuzzy linear controllers performing similar a summation.

Table 6 - Parameters of MRAC with PID Compensator

Controller	K_p	$1/T_i$	T_d
FP	$GE * GU$		
FInc	$GCE * GCU$	GE/GCE	
FPD	$GE * GU$		GCE/GE
FPD+I	$GE * GU$	GIE/GE	GCE/GE

3.6.1 Fuzzification

This transforms the data input into appropriate language values. There are two inputs to the controller, as depicted in Figure 13: error (shown in figure 13 a) and rate change of the error signals (shown in figure 13 b). The linguistic labels for the system under consideration are "Negative Big, Negative small, Zero, Positive small, Positive Big," and the universe of discourse for both e(t) and e(t) may be normalised from [-1,1]. The rules bases refer to these as "NB, NS, ZE, PS, PB." The outputs' linguistic designations are NB, NS, ZE, PS, and PB, and these labels are used in the rules bases as well [67]. The memberships of the output fuzzy logic control are publicized in Figure 14.

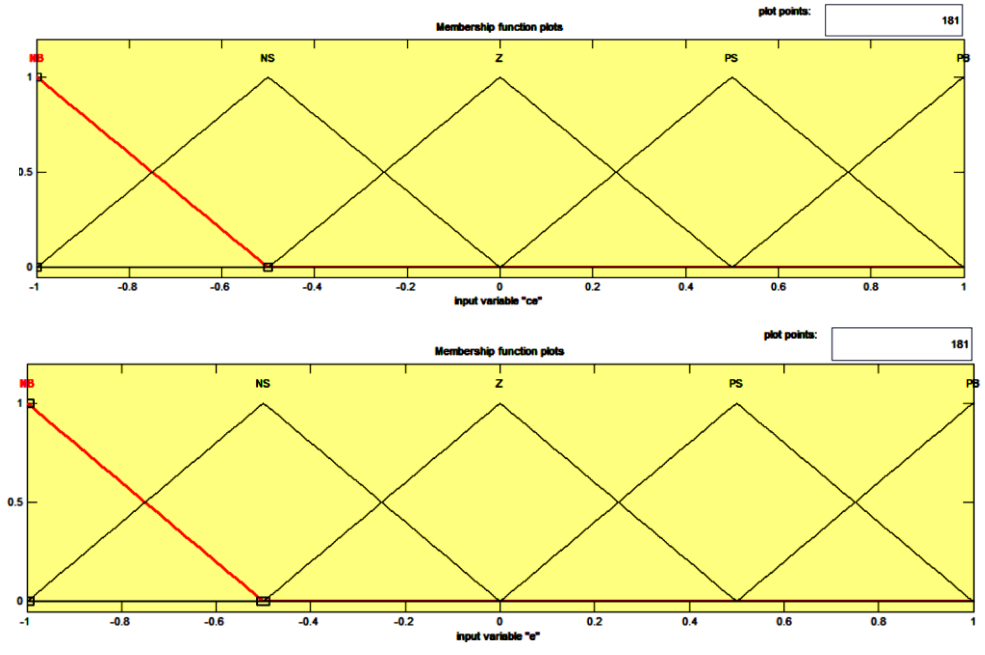

Fig. 13 - the input membership for fuzzy PD+I control.

Future Engineering Journal 2 (2022) 2314-7237

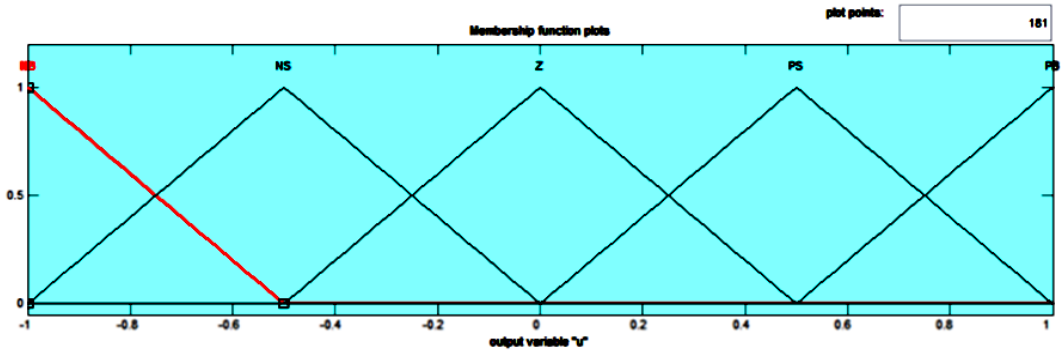

Fig. 14 - The output membership for fuzzy PD+I control.

3.6.2 Rule Base

A judgement-creation logic simulates a human decision procedure. The rule base is simplified in Tables 7. The input e has 5 language labels and Δe has 5 linguistic labels. Then we have 5×5 = 25 rule base.

Table 7 - The Rule base.

U(t)		Ce(t)				
		NB	NS	Z	PS	PB
e(t)	NB	NB	NB	NS	NS	Z
	NS	NB	NS	NS	Z	PS.
	Z	NS	NS	Z	PS	PS
	PS	NS	Z	PS	PS	PB
	PB	Z	PS	PS	PB	PB

3.6.3 Defuzzification

Defuzzification's goal is to turn a fuzzy output into a crisp value that may be used as a non-fuzzy control action. There are numerous approaches to defuzzification. The center of gravity, as shown in equation (68) [69], has been used as the defuzzification strategy in this thesis.

$$u(nT) = \frac{\sum_{j=1}^{n} u(u_j)u_j}{\sum_{j=1}^{n} u(u_j)} \quad (68)$$

Where u(uj) is the element's membership grade, u(nT) is the fuzzy control output, and n is the total number of discrete values in the discourse universe. The limitation on how much the PID controller settings can be altered is a downside of self-tuning fuzzy PID control. To ensure good performance for the Pantograph mechanism in this thesis, we shall use adaptive control. Table 8. lists below the parameters for the fuzzy PD + I controller.

Table 8 - Fuzzy Parameters

Fuzzy PD + I Parameters	GE	GCE	GIE	GU
	35	2	5	6

4. Results and Discussion:

This section displays a comparative study of the proposed control techniques executed on the pantograph mechanism.

The required path for the end-effector is a rectangle which is shown in figure 15 the profile has four corners as follows: home position (-0.1 , 0.373) , starter point (-0.05 , 0.36) , first corner (-0.05 , 0.35) , second corner (-0.14 , 0.35) , third corner (-0.14 , 0.25) , fourth corner (-0.05 , 0.25). The corresponding X & Y coordinates are shown in figure 16 which are added to the model by using Signal Builder (MATLAB Simulink).

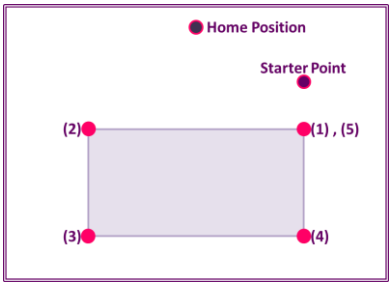

Fig. 15 -Require Coordinates.

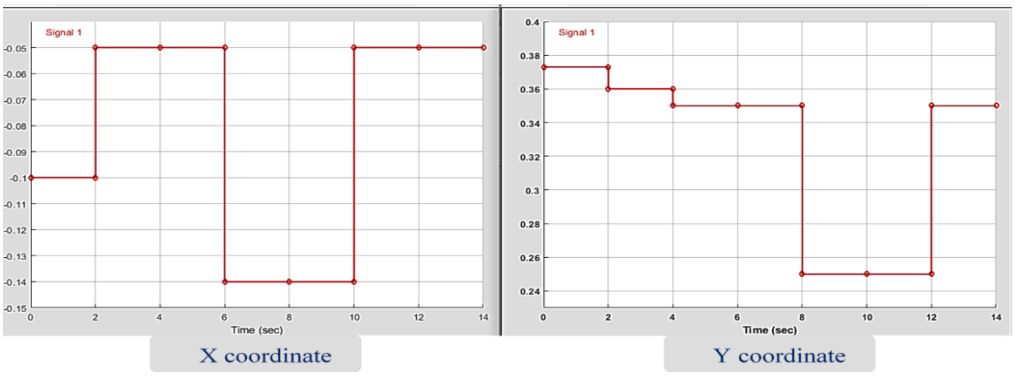

Fig. 16 - Corresponding X & Y coordinates.

4.1 Trajectory Planning with No Load

In the beginning, a comparative study between PID, FOPID, and NLPID will be implemented. The best one of them will be used to compare it with MRAC with PID compensator and Fuzzy PD+I control.

4.1.1 Comparative Study between PIDs Family

Figure 17 shows the dynamic response of θ1 and θ4 for each control technique applied on the pantograph model. It can be noted that the FOPID has a bad response because it has a high steady-state error, it reaches to the desired point tardy. The PID controllers suffer from steady-state error. The NLPID has a faster response compared to the FP-based FOPID moreover, it has a little small overshoot and undershoot.

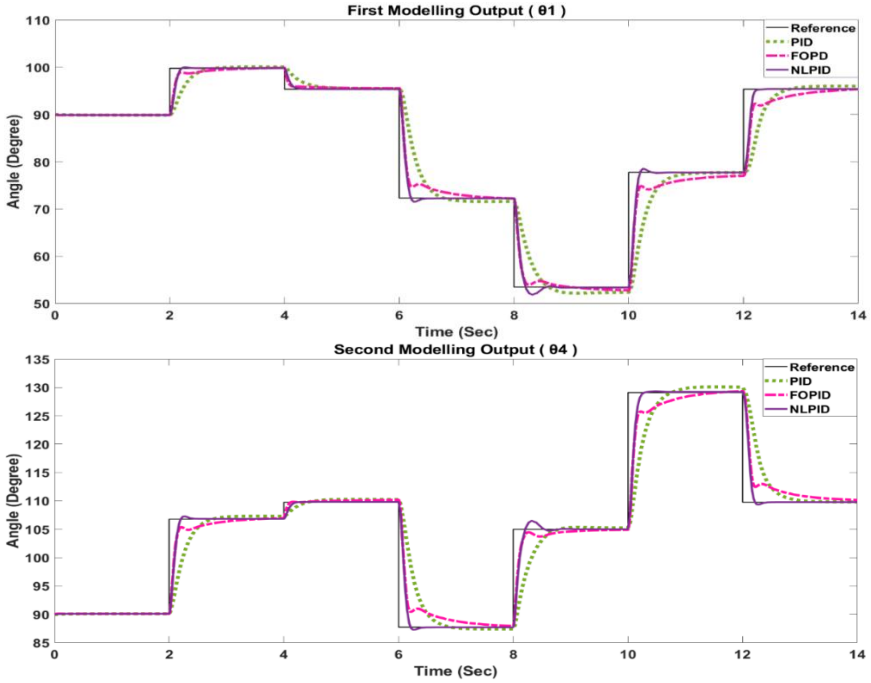

Fig. 17 - The position response of θ1 and θ4 through the PIDs Family control techniques.

Figure 19 demonstrates the corresponding velocity responses of θ1 and θ4 respectively for control techniques. It is noted that the velocity of the PID controller has a poor response, where the rise time is very large as presented in previous figure 18. The FOPID control makes the joints accelerate at a

suitable time at each change of references angle, also at backward to decays until zero rad/sec. So, the FOPID has no overshoot and undershoot as figure 18. On another side, the NLPID control has a high velocity at each new point, but its decay rapidly comparing to the FOPID controller. So, it reaches to the reference angle before the FOPID controller

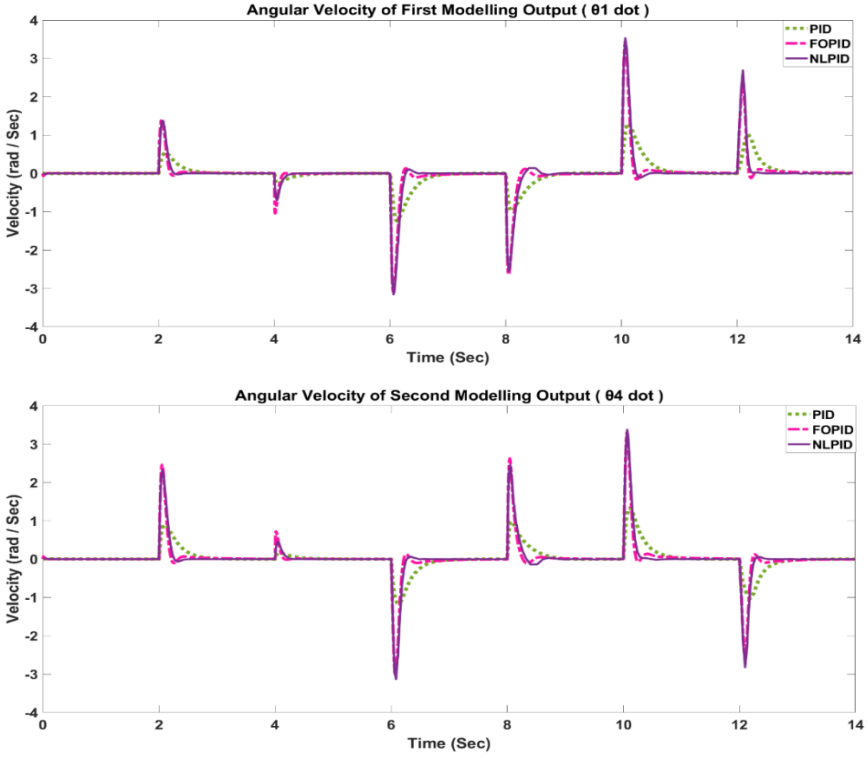

Fig. 18 -The velocity of both modeling output, velocity of θ1 and θ4 respectively, both as rad/s.

Figure 19 illustrates the corresponding output torque of PID's Family controllers. It is clear that the FOPID generates a high torque compared to the PID and NLPID controllers, with high velocity displayed in figure 19, despite that the settling time is very large, as displayed in figure 19. Moreover, the NLPID achieves a medium torque between PID and FOPID. So, it has the best performance. The PID controller has a small torque peak.

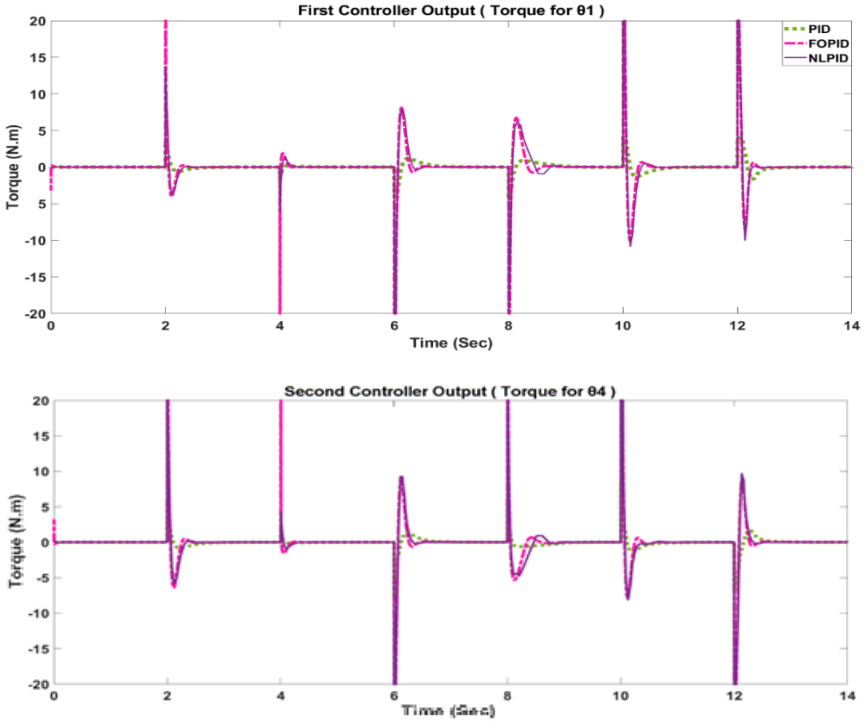

Fig. 19 - The controller output (torque N.m) is shown for the first and second controllers respectively.

Future Engineering Journal 2 (2022) 2314-7237

Figure 20 displays the trajectory planning of controllers. It is clear that the FP-based NLPID controller is more close to the reference trajectory with little overshoot at point A of the corners, it has a high accuracy compared to the FP-based FOPID and PID controller. FOPID does not reach to the desired specific points A and B. Also, it can be noted that high deviation for all controllers through the transition from horizontal line to vertical line due to the sharp corner.

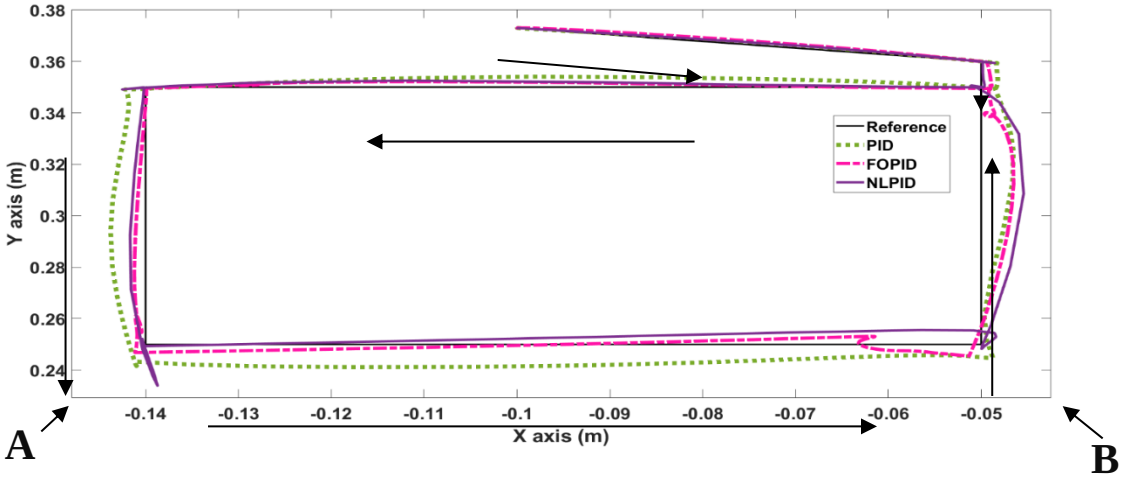

Fig. 20 - the trajectory planning of PIDs family control technics.

Figure 21 displays the trajectory planning errors of each control technique. The PID control takes a long time to absorb the error. The FOPID has a high decay for error with no undershoot and overshoot which caused an inaccuracy in the pantograph end-effector. The NLPID has the smallest time to absorb the error and it is reduced to zero error before any other control techniques so, it has the best performance. Also, the mean square error value of the proposed control techniques has been demonstrated in table 9 and 10.

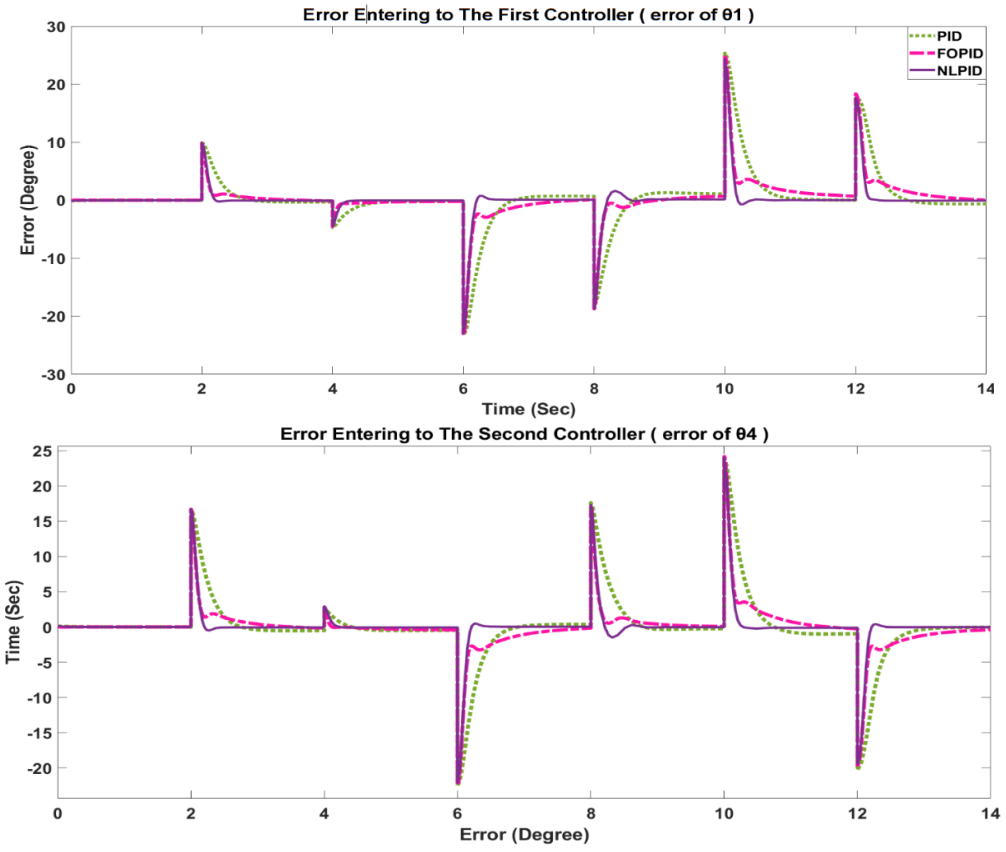

Fig. 21 -The entering error to the controller is shown for the first controller and the second one respectively.

Table 9 demonstrates the performance of the pantograph by using the PID controller, NLPID, and FOPID controller for the designed angle at each controller (θ_1 & θ_4) compared to actual.

Table 10 demonstrates the performance of the pantograph by using the PID controller, NLPID, and FOPID controller through the trajectory planning path of the end-effector, which is presented as four corners, analyzed on X-axis and Y-axis to display the extent of their conformity with the design to be implemented.

Table 9: Average of root mean square error of actual angles (θ_1 & θ_4) at each controller compared to the desire in Degree.

	PID	FOPID	NLPID
Theta 1 (θ_1)	3.8	0.96	0.90
Theta 4 (θ_4)	3.50	0.872	0.673

Table 10: Average of root mean square error of actual coordinates (X & Y) at each controller compared to the desire in cm

	PID	FOPID	NLPID
X coordinates	0.39	0.27	0.039
Y coordinates	1.93	0.309	0.117

It is worth noting here that there is a clear difference between the value of the errors in the angles (θ_1 & θ_4) and the coordinates of the points of the end-effector, the reason for this is the location of the controllers on the joints (angles θ_1 & θ_4).

After evaluating the results presented previously, it was found that the preference for the nonlinear (NLPID) controller. It has the least error and low overshoot, and it is the fastest among others to reach the design.

So, the NLPID controller will be used to compare it with advanced intelligent control techniques. The first proposed controller is the MRAC with PID Compensator, the second controller presents an intelligent control, where it uses the Fuzzy PD+I logic control techniques. All tests performed before will be applied again to investigate the best controller and improve the dynamic performance and accuracy of the pantograph. Also, the parameters for the proposed controllers will be obtained based on flower pollination

4.1.2 A Comparative Study between NLPID, Fuzzy PD+I, and MRAC with PID Compensator

Figure 22 shows the dynamic response of θ1 and θ4 respectively for each improved control techniques to the pantograph model. It can be noted the NLPID is the latest to catch up with the designed angle compared to the Fuzzy PD+I and MRAC with PID compensator and has a little overshoot. The Fuzzy PD+I controllers have very little overshot without undershoot. While MRAC with PID compensator controller has no overshoot response compared to the NLPID, and Fuzzy PD+I controllers, it resumed to the desired angle rapidly before other techniques. Accordingly, the best performance is the MRAC with PID compensator.

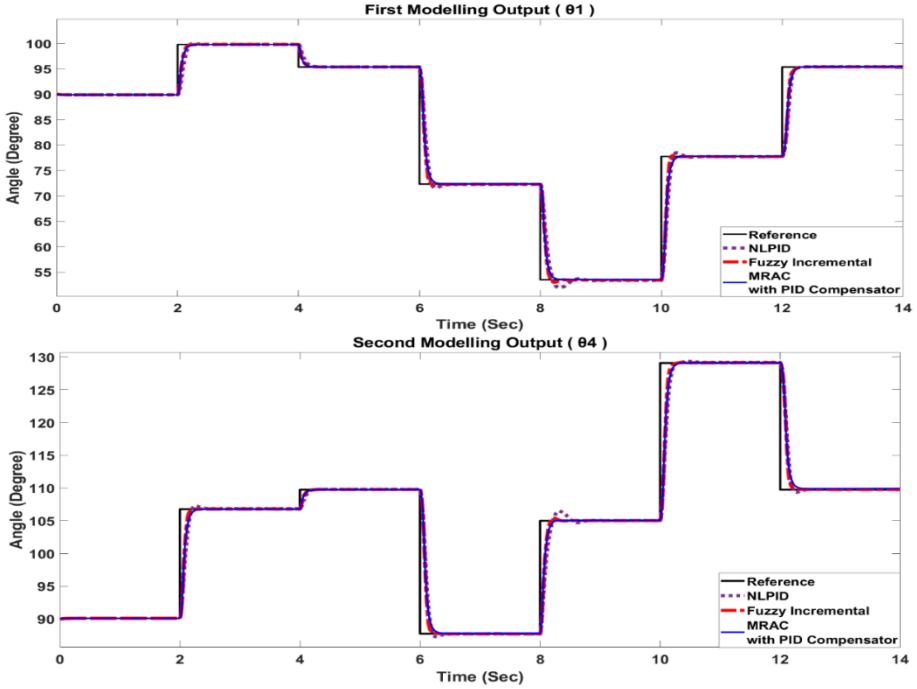

Fig. 22 - The position response of θ1 & θ4 through NLPID, Fuzzy PD+I, & MRAC techniques.

Figure 23 demonstrates the corresponding velocity responses of θ1 and θ4 respectively for control techniques. It is obvious that the MRAC has the highest velocity response compared to the others, this velocity is the reason for the performance speed occurs in the dynamic response shown before in figure 23. NLPID and Fuzzy PD+I have lower velocity, which makes them lag beside MRAC with PID compensator, as shown in figure 23. The MRAC with PID compensator Controller has a higher velocity which makes it has a faster dynamic response with no disturbance shown in figure 22.

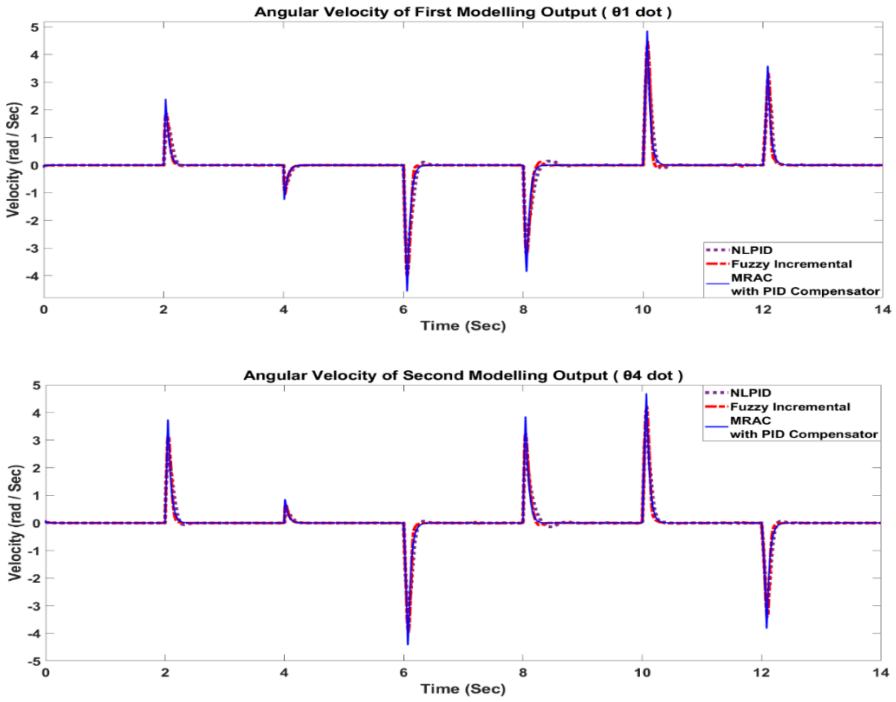

Fig. 23 - The position response of θ1 and θ4 through NLPID, Fuzzy PD+I, and MRAC, Control.

Figure 24 illustrates the corresponding output torque of controllers. It is obvious that the NLPID controller has a small torque peak, which makes it slow. The Fuzzy PD+I has medium torque in a small period, which makes it have a little overshoot. While MRAC generates a higher torque compared to the NLPID and Fuzzy PD+I controllers, which is the real reason for the high velocity at an appropriate time, thus the occurrence of a high-speed response without overshoot.

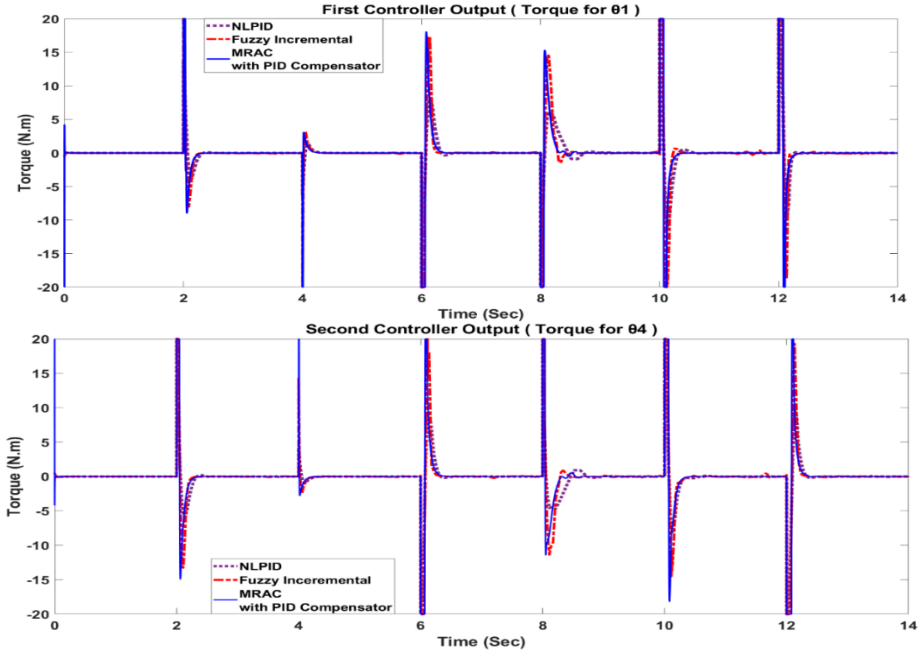

Fig. 24 -The controller output (torque N.m) is shown for the first and second controller respectively for NLPID ,Fuzzy PD+I, and MRAC with PID Compensator.

Figure 25 displays the controllers' trajectory planning for the end-effector. It is clear thus the proposed controllers NLPID and Fuzzy PD+I have an overshoot for θ_1 and θ_4 , will give high vibration at corners of trajectory profile. Where the MRAC Compensator with PID controller has no disturbance, while NLPID is highest and Fuzzy PD+I is lower. So, the MRAC with PID compensator controller has higher accuracy compared to other controllers.

Also, it can be noted that high deviation for all controllers through the transition from horizontal lines to vertical lines due to the sharp corners, but in MRAC with PID compensator has no disturbance in sharp corners.

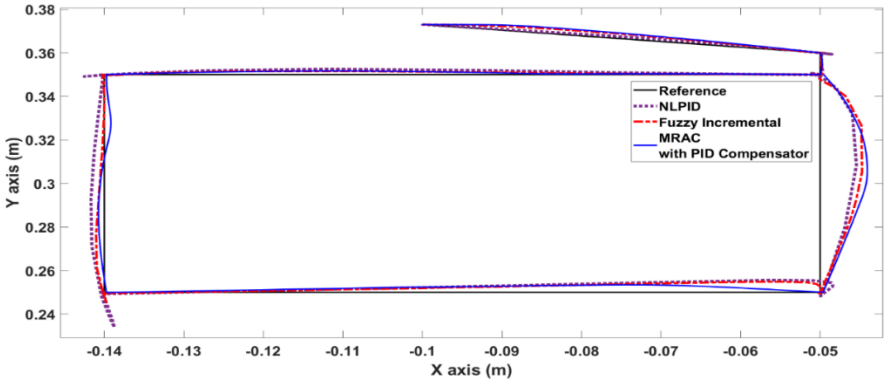

Fig. 25 - The trajectory planning of NLPID, Fuzzy PD+I, and MRAC with PID compensator control technics.

Figure 26 displays the trajectory planning errors of three control techniques. In the beginning, the simulation controller errors are equal. It noted the error of each control is high at every new operating point. The performance of each control depends on the minimum time to reach zero error with the lowest overshoot and undershoot. The NLPID has the highest overshoot and undershoot. Fuzzy PD+I has a lower time than NLPID, but it is having a little overshoot and undershoot. The (MRAC) with PID compensator has a lower time to dampen the error compared to the other controllers without overshoot or undershoot. Also, the mean square error value of the proposed control techniques has been demonstrated in tables 11 and 12 below.

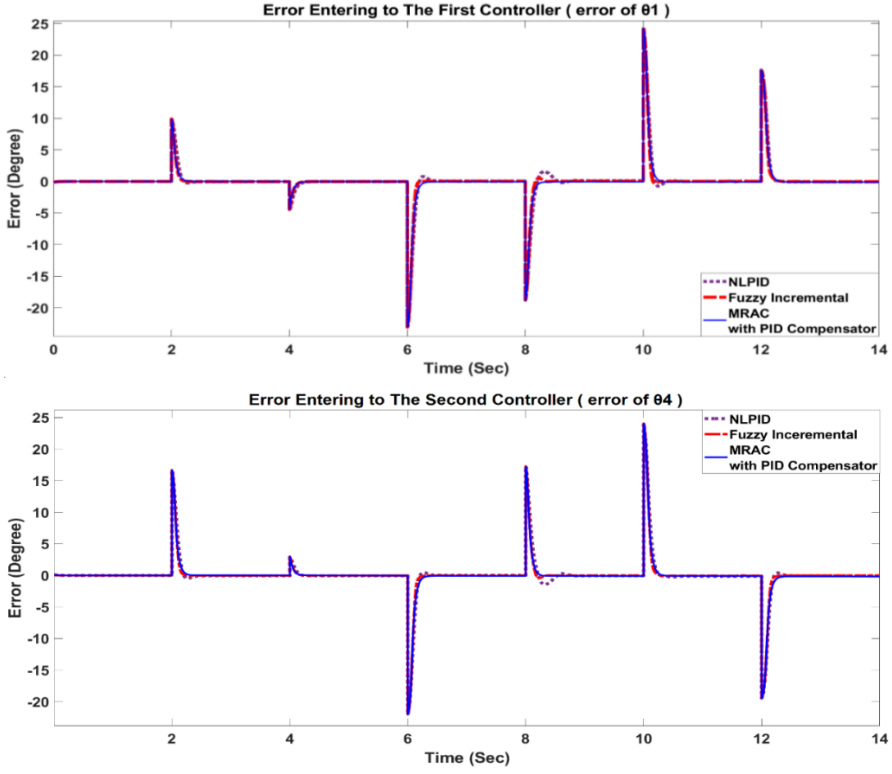

Fig. 26 - The entering error to the controller is shown for the first controller and the second one respectively.

Table 11 demonstrates the performance of the pantograph by using the NLPID, Adaptive Control with PID Compensator, and Fuzzy PD+I control for the designed angle at each controller (θ_1 & θ_4) compared to actual.

Table 12 demonstrates the performance of the pantograph by using the NLPID, MARC with PID Compensator, and Fuzzy PD+I control through the trajectory planning path at the end-effector, which is presented as four corners, analyzed to X-axis and Y-axis to display the extent of their conformity with the design to be implemented.

Table 11: Average root mean square error of Actual angles (θ_1 & θ_4) at each controller compared to the desired.

	MRAC with PID compensator	NLPID	FUZZY PD+I
Theta 1 (θ_1)	0.06°	0.90°	0.17°
Theta 4 (θ_4)	0.047°	0.673°	0.15°

Table 12: Average root mean square error of actual coordinates (X & Y) at each controller compared to the desired.

	MRAC with PID Compensator	NLPID	FUZZY PD+I
X coordinates	0.010 cm	0.039 cm	0.011 cm
Y coordinates	0.014 cm	0.117 cm	0.13 cm

It is worth noting here that there is a clear difference between the percentage of the errors in the angles (θ_1 & θ_4) and the coordinates of the points of the end-effector, the reason for this is the location of the controllers on the joints (angles θ_1 & θ_4).

After evaluating the results presented previously, it was found that the preference for the nonlinear (MRAC) with PID Compensator controller. It has the least error and no overshoot and undershoot, and it is the fastest among others to reach the design, obtained based on flower pollination algorithm.

4.2 Trajectory Planning with Load

After testing all proposed controllers, obvious that the best performance controllers are NLPID, Fuzzy PD+I, and MRAC. So, the trajectory planning will be applied with load to ensure the controllers unsensitivity to disturbance.

4.2.1 A Comparative Study between NLPID, MRAC & Fuzzy PD+I Control

Figure 27 shows the dynamic response of θ1 and θ4 respectively for each improved control techniques to the pantograph model under load equal 3N in X axis and 3N in Y axis.

It can be noted that the performance of each control techniques under the load is a same as no load which is presented in figure 18 above.

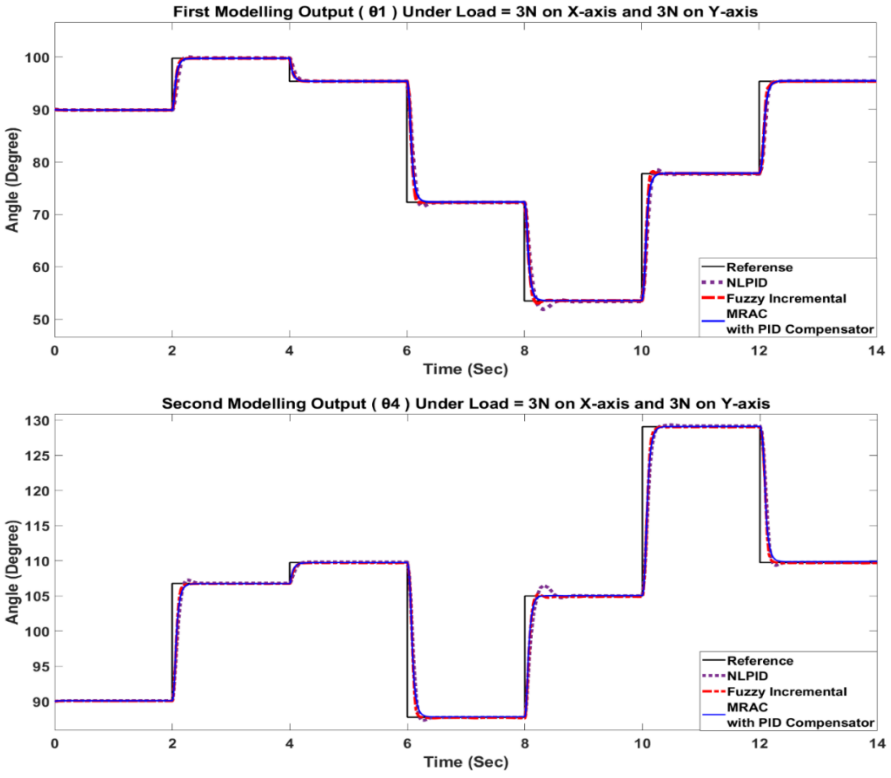

Fig. 27 - Position response of θ1 & θ4 under load, through NLPID, Fuzzy PD+I, and MRAC.

4.2.2 A Comparative Study between NLPID, MRAC & Fuzzy PD+I Control for triangle profile

Figure 28 displays the controllers' trajectory planning for end-effector under load, which is equal 3N at X axis and 3N at Y axis. It is clear thus the proposed controllers NLPID, Fuzzy PD+I, and MRAC with PID compensator have a same performance as no load.

The MRAC compensator with PID controller has no disturbance, it has the highest accuracy compared to other controllers.

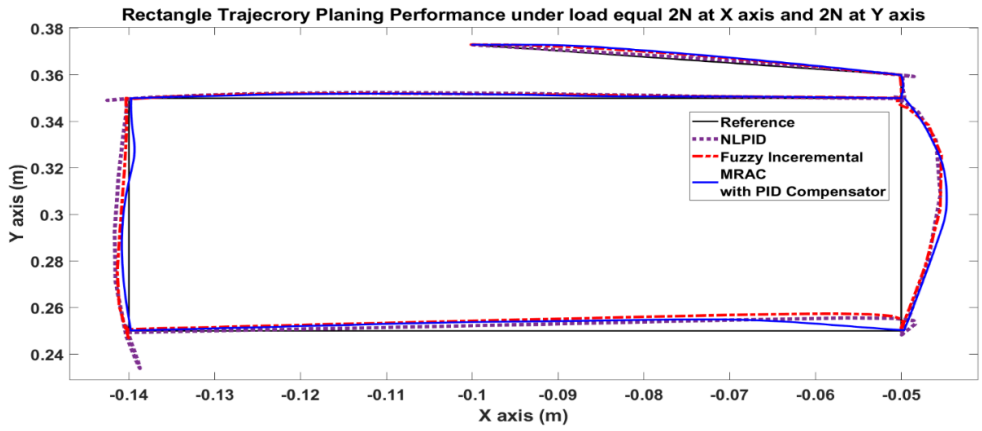

Fig. 28 -: The trajectory planning of NLPID, Fuzzy PD+I, and MRAC with PID compensator control technics.

5 Conclusion

In this work, a verified mathematical model for Pantograph Robot Mechanism had been developed where the boundary conditions are taken into account. Also, an advanced intelligent control techniques had been implemented to increase the performance of the Pantograph Robot Mechanism. The first control technique is the famous PID controller which has a simple structure but it considers a linear controller. So, it suffers from a poor performance for nonlinear systems as occurred in the Pantograph Robot Mechanism. The second control technique is fractional order PID controller which considers the other face of PID control in a nonlinear form. It achieved a satisfied response when it applied on the Pantograph Robot Mechanism compared to the PID controller. The third controller is a new enhanced nonlinear PID (NPID) controller which has a hybrid gain consists of linear and nonlinear parts. A comparative study had been implemented to find the best performance among the PID's family controllers. The NPID had achieved the best performance compared to the PID and FOPID controllers. The fourth controller is the model reference adaptive with PID compensator which can absorb the nonlinearity and the system disturbances as demonstrated in the results. The fifth controller is an intelligent fuzzy PD+I controller where the fuzzy logic system has the flexibility to manage the sudden disturbances fastly and nonlinear behavior as illustrated in the results. Moreover, the proposed control techniques were designed and optimized by Flower Pollination (FP) algorithm optimization. A rectangular trajectory was selected to be a position reference of the end effector of the pantograph robot, which gives a more accurate study because it shows performance during sharp edges. This task was done using the proposed controllers to investigate the performance. The results show that the Fuzzy PD+I control has a better performance compared to the PID, FOPID, NLPID, and MRAC with PID Compensator controllers.

References

[1] Jorge Angeles, "Fundamentals of Robotic Mechanical Systems: Theory, Methods, and Algorithms," *Springer, New York.*, 2007.

[2] M. Raibert, "BigDog, the rough-terrain quadruped robot," in *IFAC Proceedings Volumes (IFAC-PapersOnline)*, 2008, vol. 17, no. 1 PART 1. doi: 10.3182/20080706-5-KR-1001.4278.

[3] *2008 IEEE Workshop on Advanced Robotics and its Social Impacts.* I E E E, 2008.

[4] Y. Xu and H. bin Wang, "Flying robot with undulating wings," in *IFAC Proceedings Volumes (IFAC-PapersOnline)*, 2013, vol. 2, no. PART 1, pp. 181–186. doi: 10.3182/20131120-3-FR-4045.00017.

[5] J. Hodgins, "H-Delta: Design and Applications of a Novel 5 Degree of Freedom Parallel Robot," 2018.

[6] M. Arns, "Novel reconfigurable Delta Robot dual-functioning as Adaptive Landing Gear and Manipulator," 2019.

[7] "The Shuttle Remote Manipulator System -- The Canadarm," *https://www.ieee.ca/millennium/canadarm/canadarm_technical.html*, 2019.

[8] A. Gasparetto and L. Scalera, "A Brief History of Industrial Robotics in the 20th Century," *Advances in Historical Studies*, vol. 8, pp. 24–35, 1950, doi: 10.4236/cm.2019.81002.

[9] Zhongxing Yang "Novel Design and Analysis Of Parallel Robotic Mechanisms," thesis doctor of philosophy, York university, 2019.

[10] J. Yamine, A. Prini, M. Lavit Nicora, T. Dinon, H. Giberti, and M. Malosio, "A planar parallel device for neurorehabilitation," *Robotics*, vol. 9, no. 4, pp. 1–22, Dec. 2020, doi: 10.3390/robotics9040104.

[11] B. Wei, "Performance Improvement for Robotic Mechanisms by: Synthesis Design, Dynamic Balancing and Adaptive Control Techniques," 2016.

[12] H. Cervantes-Culebro, J. E. Chong-Quero, E. A. Padilla-Garcia, and C. A. Cruz-Villar, "Concurrent Design of a 2 Dof Five-Bar Parallel Robot a Hybrid Design of Rigid and Flexible Links," *IEEE Access*, vol. 9, pp. 17450–17462, 2021, doi: 10.1109/ACCESS.2021.3053250.

[13] V. Nabat, M. de La O Rodriguez, O. Company, S. Krut, and F. Pierrot, "Par4: Very high speed parallel robot for pick-and-place," in *2005 IEEE/RSJ International Conference on Intelligent Robots and Systems, IROS*, 2005, pp. 553–558. doi: 10.1109/IROS.2005.1545143.

[14] Christine Connolly "ABB high-speed picking robots establish themselves in food packaging," *Industrial Robot*, vol. 34, no. 4, pp. 281–284, 2007, doi: 10.1108/01439910710749591.

[15] J. P. Merlet, "Parallel robots," *Solid Mechanics and its Applications*, vol. 128, pp. 1–413, 2006, doi: 10.1007/978-3-319-72911-4_6.

[16] E. L. J. Bohez, "Five-axis milling machine tool kinematic chain design and analysis," 2002.

[17] M.-S. Tsai, T.-N. Shiau, Y.-J. Tsai, and T.-H. Chang, "Direct kinematic analysis of a 3-PRS parallel mechanism." [Online]. Available: www.elsevier.com/locate/mechmt

[18] P. Wenger, D. C. Chablat, F. Majou, and D. Chablat, "Design of a 3 Axis Parallel Machine Tool for High Speed Machining: The Orthoglide Design and analysis of a new 'Elephant trunk' type robot for piping inspection View project Contribution to dynamic modeling, identification and control of parallel robots View project DESIGN OF A 3 AXIS PARALLEL MACHINE TOOL FOR HIGH SPEED MACHINING : THE ORTHOGLIDE," 2007. [Online]. Available: https://www.researchgate.net/publication/1889601

[19] E. Kljuno and R. L. W. Ii, "Vehicle Simulation System: Controls and Virtual-Reality-Based Dynamics Simulation," 2008.

[20] M. Suciu, B. Gherman, C. Vaida, N. Plitea, A. Stoica, and D. Pisla, "On the kinematics of a hybrid parallel robot used in minimally invasive surgery," in *Mechanisms and Machine Science*, 2012, vol. 3, pp. 255–262. doi: 10.1007/978-94-007-2727-4_23.

[21] S. Lessard, P. Bigras, and I. A. Bonev, "A new medical parallel robot and its static balancing optimization," *Journal of Medical Devices, Transactions of the ASME*, vol. 1, no. 4, pp. 272–278, Dec. 2007, doi: 10.1115/1.2815329.

[22] B. Gherman, N. Plitea, and D. Pisla, "An innovative parallel robotic system for transperineal prostate biopsy," in *Mechanisms and Machine Science*, 2017, vol. 43, pp. 421–429. doi: 10.1007/978-3-319-44156-6_43.

[23] F. Xi, A. Ross, and S. Lang, "Exploring a Re-configurable Parallel Robot for Space Applications," St-Hubert, 2001.

[24] T. P. Jones and G. R. Dunlop, "Analysis of rigid-body dynamics for closed-loop mechanisms-its application to a novel satellite tracking device," 2003.

[25] D. Zhang, Z. Gao, and I. Fassi, "Design optimization of a spatial hybrid mechanism for micromanipulation," *International Journal of Mechanics and Materials in Design*, vol. 7, no. 1, pp. 55–70, Mar. 2011, doi: 10.1007/s10999-011-9149-3.

[26] Y. Tian, B. Shirinzadeh, D. Zhang, X. Liu, and D. Chetwynd, "Design and forward kinematics of the compliant micro-manipulator with lever mechanisms," *Precision Engineering*, vol. 33, no. 4, pp. 466–475, Oct. 2009, doi: 10.1016/j.precisioneng.2009.01.003.

[27] B. Zi, J. Cao, and Z. Zhu, "Dynamic Simulation of Hybrid-driven Planar Five-bar Parallel Mechanism Based on SimMechanics and Tracking Control Regular Paper." [Online]. Available: www.intechopen.com

[28] A. Mizrain and R. Garcia, "'MODELING, INDENTIFICATION AND ANALISYS OF THE DYNAMIC BEHAVIOR OF RECONFIGURABLE PARALLEL ROBOT' Dual Program Master in Optomechatronics from Centro de Investigaciones en Óptica Internship conducted at."

[29] S. Jian, S. John, C. Cheng Yin, C. Luc Rolland, and C. Lesley James, "FIVE BAR PLANAR MANIPULATOR SIMULATION AND ANALYSIS BY BOND GRAPH," 2014. [Online]. Available: http://www.asme.org/about-asme/terms-of-use

[30] H. Cervantes-Culebro, J. E. Chong-Quero, E. A. Padilla-Garcia, and C. A. Cruz-Villar, "Concurrent Design of a 2 Dof Five-Bar Parallel Robot a Hybrid Design of Rigid and Flexible Links," *IEEE Access*, vol. 9, pp. 17450–17462, 2021, doi: 10.1109/ACCESS.2021.3053250.

[31] Z. Saeed, B. Gabra, M. Sallam, W. Refeay, and S. Sharaf, "Modeling and Control of a Pantograph Mechanism Interacting with the Environment," in *Advances in Intelligent Systems and Computing*, 2021, vol. 1339, pp. 717–726. doi: 10.1007/978-3-030-69717-4_67.

[32] S. Karande, P. S. v Nataraj, P. S. Gandhi, and M. M. Deshpande, "Control of Parallel Flexible Five Bar Manipulator using QFT."

[33] X. Yang *et al.*, "Modified Robust Dynamic Control for a Diamond Parallel Robot," *IEEE/ASME Transactions on Mechatronics*, vol. 24, no. 3, pp. 959–968, Jun. 2019, doi: 10.1109/TMECH.2019.2914165.

[34] Viện khoa học và công nghệ Việt Nam, Đại học quốc gia TP. Hồ Chí Minh, IEEE Vietnam Section, and Institute of Electrical and Electronics Engineers, *2013 International Conference on Control, Automation and Information Sciences (ICCAIS)*.

[35] Louis Vathan.B, Hoshila Kumar and Brighton Issac John.H "Kinematic_Analysis_of_Five_Bar_Mechanism". Academia, 2016.

[36] B. Zi, J. Cao, and Z. Zhu, "Dynamic Simulation of Hybrid-driven Planar Five-bar Parallel Mechanism Based on SimMechanics and Tracking Control Regular Paper." [Online]. Available: www.intechopen.com

[37] G. Campion, S. Member, Q. Wang, V. Hayward, and S. Member, "The Pantograph Mk-II: A Haptic Instrument *." [Online]. Available: www.cim.mcgill.ca/~haptic

[38] X. Cano-Ferrer, "Educational Five-Bar Parallel Robot."

[39] C. Gallacher, J. Willes, and J. Kovecses, "Parasitic effects of device coupling on haptic performance," in *IEEE World Haptics Conference, WHC 2015*, Aug. 2015, pp. 266–272. doi: 10.1109/WHC.2015.7177724.

[40] J. Wang, C.M. Gosselin, and L. Cheng, "Modeling and simulation of robotic systems withclosed kinematic chains using the virtual spring approach,"Multibody System Dynamics,vol. 7, no. 2, pp. 145–170, 2002.7

[41] S. Karande, P. S. v Nataraj, P. S. Gandhi, and M. M. Deshpande, "Control of Parallel Flexible Five Bar Manipulator using QFT."

[42] F. Cemal and H. Şen, "Real time controlled two dof five bar robot manipulator," 2017.

[43] R. Hosseinzadeh and M. Zarebnia, "Application and comparison of the two efficient algorithms to solve the pantograph Volterra fuzzy integro-differential equation," *Soft Computing*, vol. 25, no. 10, pp. 6851–6863, May 2021, doi: 10.1007/s00500-021-05691-8.

[44] S. Kosari, Z. Shao, M. Yadollahzadeh, and Y. Rao, "Existence and Uniqueness of Solution for Quantum Fractional Pantograph Equations," *Iranian Journal of Science and Technology, Transaction A: Science*, vol. 45, no. 4, pp. 1383–1388, Aug. 2021, doi: 10.1007/s40995-021-01124-1.

[45] J. W. Yoon, J. Ryu, and Y. K. Hwang, "Optimum design of 6-DOF parallel manipulator with translational/rotational workspaces for haptic device application," *Journal of Mechanical Science and Technology*, vol. 24, no. 5, pp. 1151–1162, May 2010, doi: 10.1007/s12206-010-0321-8.

[46] C. M. Pappalardo, M. C. de Simone, and D. Guida, "Multibody modeling and nonlinear control of the pantograph/catenary system," *Archive of Applied Mechanics*, vol. 89, no. 8, pp. 1589–1626, Aug. 2019, doi: 10.1007/s00419-019-01530-3.

[47] C. M. Pappalardo, M. C. De Simone, and D. Guida, "Multibody modeling and nonlinear control of the pantograph/catenary system," *Archive of Applied Mechanics*, vol. 89, no. 8, pp. 1589–1626, 2019, doi: 10.1007/s00419-019-01530-3.

[48] Z. Sabir, M. A. Z. Raja, D.-N. Le, and A. A. Aly, "A neuro-swarming intelligent heuristic for second-order nonlinear Lane–Emden multi-pantograph delay differential system," *Complex & Intelligent Systems*, May 2021, doi: 10.1007/s40747-021-00389-8.

[49] X. Cano-Ferrer, "Educational Five-Bar Parallel Robot."

[50] Institute of Electrical and Electronics Engineers., *ICRA 2012 : 2012 IEEE International Conference on Robotics and Automation : St. Paul, Minnesota, USA, May 14-18, 2012.* [IEEE], 2012.

[51] R. S. Umamaheswara Raju, V. V. S. S. S. Chakravarthy, and P. S. R. Chowdary, "Flower pollination algorithm based reverse mapping methodology to ascertain operating parameters for desired surface roughness," *Evolutionary Intelligence*, vol. 14, no. 2, pp. 1145–1150, 2021, doi: 10.1007/s12065-021-00574-1.

[52] A. A. E.-S. Adel A. A. El-Gammal, "Adaptive Tuning of a PID Speed Controller For DC Motor Drives Using Multi-Objective Particle Swarm Optimization MOPSO," 2009.

[53] N. A. Elkhateeb and R. I. Badr, "Novel PID Tracking Controller for 2DOF Robotic Manipulator System Based on Artificial Bee Colony Algorithm," *Electrical, Control and Communication Engineering*, vol. 13, no. 1, pp. 55–62, 2017, doi: 10.1515/ecce-2017-0008.

[54] M. A. Shamseldin, M. Sallam, A. M. Bassiuny, and A. M. A. Ghany, "A new model reference self-tuning fractional order PD control for one stage servomechanism system," *WSEAS Transactions on Systems and Control*, vol. 14, pp. 8–18, 2019.

[55] Mohamed Shamseldin, "Speed Control of High Performance Brushless DC Motor," 2016, doi: 10.13140/RG.2.1.1472.9202.

[56] V. Chopra, S. K. Singla, and L. Dewan, "Comparative Analysis of Tuning a PID Controller using Intelligent Methods."

[57] P. H. Krishnan and M. Arjun, "Control of BLDC Motor Based on Adaptive Fuzzy Logic PID Controller."

[58] S. A. Deraz, "Genetic Tuned PID Controller Based Speed Control of DC Motor Drive," *International Journal of Engineering Trends and Technology*, vol. 17, no. 2, 2014, [Online]. Available: http://www.ijettjournal.org

[59] Y. X. Su, D. Sun, and B. Y. Duan, "Design of an enhanced nonlinear PID controller," *Mechatronics*, vol. 15, pp. 1005–1024, 2005, doi: 10.1016/j.mechatronics.2005.03.003.

[60] S. B. U, "Multivariable Centralized Fractional Order PID Controller tuned using Harmony search Algorithm for Two Interacting Conical Tank Process," in *SAI Intelligent Systems Conference 2015 November 10-11, 2015 | London, UK Multivariable*, 2015, pp. 320–327.

[61] P. Zhao and Y. Shi, "Robust control of the A-axis with friction variation and parameters uncertainty in five-axis CNC machine tools," *Journal of Mechanical Engineering Science*, 2014, doi: 10.1177/0954406213519759.

[62] B. B. Reddy, "Modelling and Control of 2-DOF Robotic Manipulator Using BLDC Motor," *International Journal of Science, Engineering and Technology Research (IJSETR), Volume 3, Issue 10, October 2014 Modelling*, vol. 3, no. 10, pp. 2760–2763, 2014.

[63] M. A. A. Ghany, M. A. Shamseldin, and A. M. A. Ghany, "A Novel Fuzzy Self Tuning Technique of Single Neuron PID Controller for Brushless DC Motor," *International Journal of Power Electronics and Drive System (IJPEDS)*, vol. 8, no. 4, pp. 1705–1713, 2017, doi: 10.11591/ijpeds.v8i4.pp1705-1713.

[64] P. Swarnkar, S. Jain, and R. K. Nema, "Effect of Adaptation Gain in Model Reference Adaptive Controlled Second Order System," 2011. [Online]. Available: www.etasr.com

[65] M. A. Shamseldin, M. Abdullah Eissa, and A. A. El-Samahy, "A Modified Model Reference Adaptive Controller for Brushless DC Motor."

[66] P. Jain and M. J. Nigam, "Design of a Model Reference Adaptive Controller Using Modified MIT Rule for a Second Order System," 2013. [Online]. Available: http://www.ripublication.com/aeee.htm

[67] U. Kumar Bansal and R. Narvey, "Speed Control of DC Motor Using Fuzzy PID Controller," 2013. [Online]. Available: http://www.ripublication.com/aeee.htm

[68] Y. R.M.Kuraz and M. M.F. Algreer, "Design Fuzzy Self Tuning of PID Controller for Chopper-Fed DC Motor Drive," *AL-Rafdain Engineering Journal (AREJ)*, vol. 16, no. 2, pp. 54–66, Apr. 2008, doi: 10.33899/rengj.2008.44538.

[69] N. J. Patil, Dr. R. H. Chile, and Dr. L. M. Waghmare, "Fuzzy Adaptive Controllers for Speed Control of PMSM Drive," *International Journal of Computer Applications*, vol. 1, no. 11, pp. 91–98, Feb. 2010, doi: 10.5120/233-387.